Contracting Wide-area Network Topologies to Solve Flow Problems Quickly: Extended Version

Firas Abuzaid[†*], *Srikanth Kandula*[†], *Behnaz Arzani*[†], *Ishai Menache*[†], *Matei Zaharia*[*], *Peter Bailis*[*]
Microsoft Research[†] *and Stanford University*[*]

Abstract– Many enterprises today manage traffic on their wide-area networks using software-defined traffic engineering schemes, which scale poorly with network size; the solver runtimes and number of forwarding entries needed at switches increase to untenable levels. We describe a novel method, which, instead of solving a multi-commodity flow problem on the network, solves (1) a simpler problem on a contraction of the network, and (2) a set of sub-problems in parallel on disjoint clusters within the network. Our results on the topology and demands from a large enterprise, as well as on publicly available topologies, show that, in the median case, our method nearly matches the solution quality of currently deployed solutions, but is 8× faster and requires 6× fewer FIB entries. We also show the value-add from using a faster solver to track changing demands and to react to faults.

1 Introduction

Wide-area networks (WANs), which connect locations across the globe with high-capacity optical fiber, are an expensive resource [7, 35, 36, 38]. Hence, enterprises seek to carefully manage the traffic on their WANs to offer low latency and jitter for customer-facing applications [28, 62, 69] and fast response times for bulk data transfers [46, 56].

The state-of-the-art approach used in several enterprises today [35, 36, 38] is to compute optimal routing schemes for the current demand by solving global multi-commodity flow problems [7, 35, 36, 38]; the global flow problems are re-solved periodically, since demands may change or links may fail, and the computed routes are encoded into switch forwarding tables using software-defined networking techniques [7].

As network sizes grow, solving multi-commodity flow problems on the entire network becomes practically intractable. As noted in [36], the "algorithm run time increased super-linearly with the site count," which led to "extended periods of traffic blackholing during data plane failures, ultimately violating our availability targets," as well as "scaling pressure on limited space in switch forwarding tables." This problem is unlikely to go away: anecdotal reports indicate that WAN footprints today are already over 10× larger than the few tens of sites that were considered in prior work [35, 36], since enterprises have built more sites to move closer to users.

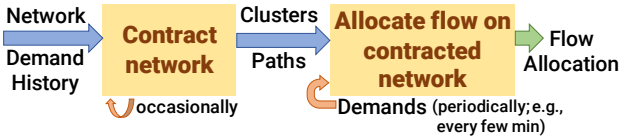

Figure 1: NCFlow's workflow.

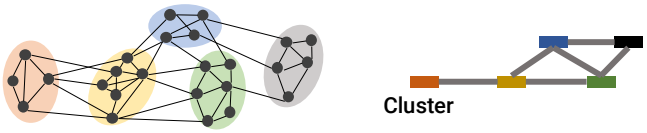

Figure 2: The original network on the left is divided into clusters, shown with different background colors. The contracted network is on the right.

In this paper, we seek to retain the benefits of global traffic management for large WAN networks without requiring excessively many forwarding entries at switches or prohibitively long solver runtimes. Also, by using a faster solver, WAN operators can reduce loss when faults occur and carry more traffic on the network by tracking demand changes.

Our solution is motivated by the observation that WAN topologies and demands are *concentrated*: the topology typically has well-connected portions separated by a few, lower-capacity edges, and more demand is between nearby datacenters. This is likely due to multiple operational considerations: (1) submarine cables have become shared choke points for connectivity between continents (see Figure 3), (2) the connectivity over land follows the road or rail networks along which fiber is typically laid out, and (3) enterprises build datacenters close to users, then steer traffic to nearby datacenters [12, 62, 69]. Therefore, more capacity and demand are available between *nearby* nodes; an analysis of data from a large enterprise WAN in §2 supports this observation.

We leverage this concentration of capacity and demand to decompose the global flow problem into several smaller problems, many of which can be solved in parallel. As shown

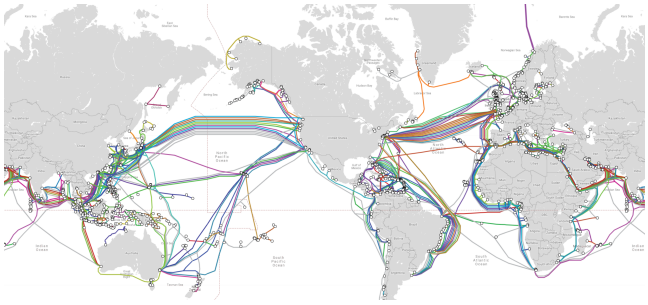

Figure 3: Submarine cables serve as choke points in WAN topologies; figure is excerpted from [63].

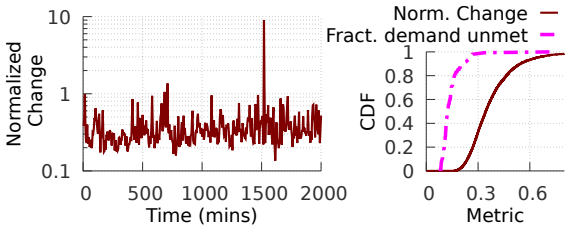

Figure 4: On the left, we plot the L2 norm of the change in the demands between successive 5-minute periods divided by the L2 norm of the traffic matrix at a time. On the right, we show the CDF of this change ratio. We also show a CDF of the fraction of demand that is unsatisfied if using the allocation computed for the previous period.

in Figure 2, we divide the network into multiple connected components, which we refer to as *clusters*. We then solve modified flow problems on each cluster, as well as on the *contracted network*, where nodes are clusters and edges connect clusters that have connected nodes. Prior work [4, 9, 15] notes that Google and other map providers use different contractions to compute shortest paths on road network graphs. Our goal is to closely match the multi-commodity max flow solution in quality (i.e., carry nearly as much total flow), while reducing the solver runtime and number of required forwarding entries. We discuss related work in §7; to our knowledge, we are the first to demonstrate a practical technique for multi-commodity flow problems on large WAN topologies.

Solving flow problems on the contracted network poses two key challenges:

1. How to partition the network into clusters? More clusters leads to greater parallelism, but maximizing the inter-cluster flow requires careful coordination between the sub-problems at multiple clusters.
2. How to design the sub-problems for each cluster to improve speed while reducing inconsistencies in allocation? The sub-problem for a cluster has fewer nodes and edges to consider, but it will not be be faster if it must consider all node pairs whose traffic can pass through the cluster.

Our solution NCFlow[1] achieves a high-quality flow allocation with a low runtime and space complexity by addressing each of these challenges in turn. First, we contract the network using well-studied algorithms such as modularity-based clustering [25] and spectral clustering [53], which are designed to identify the choke-point edges in a network. Second, we *bundle* demands whose sources and/or targets are in the same cluster, treating them as a single demand. In Figure 2 for example, the yellow cluster considers as one bundled demand all traffic from source nodes in the red cluster to target nodes in the green cluster. Doing so can lead to inconsistent flow allocations between clusters (which we explain in §3.1.1) and we devise careful heuristics to provably avoid them (§3.2). Finally, we reduce the forwarding entries needed at switches by reusing pathlets within clusters and traffic splitting rules across multiple demands (§3.5).

Figure 1 shows the workflow for NCFlow. First, we choose appropriate clusters and paths using an offline procedure over historical traffic—these choices are pushed into the switch forwarding entries. This step happens infrequently, such as when the topology and/or traffic changes substantially. Then, online (e.g., once every few minutes), NCFlow computes how best to route the traffic over the clusters and paths, similar to deployed solutions [35, 36, 38].

Overall, our key contributions are:

- We propose NCFlow, a decomposition of the multi-commodity max flow problem into an offline clustering step and an online, provably feasible, algorithm that solves a set of smaller sub-problems in parallel.
- We evaluate NCFlow using real traffic on a large enterprise WAN, as well as synthetic traffic on eleven topologies from the Internet Topology Zoo [6]. Our results show that, for multi-commodity max flow, NCFlow is within 2% of the total flow allocated by state-of-the-art path-based LP solvers [35, 36, 38] in 50% of cases; NCFlow is within 20% in 97% of cases. Furthermore, NCFlow is at least 8× faster than path-based LP solvers in the median case; in 20% of cases, NCFlow is over 30× faster. Lastly, NCFlow requires 2.7–16.7× fewer forwarding entries in the evaluated topologies. NCFlow also compares favorably to state-of-the-art approximation algorithms [27, 41] and oblivious techniques [44, 57].
- We show that, as a fast approximate solver, NCFlow can be used to react quickly to demand changes and link failures. Specifically, in comparison to TEAVAR [19], NCFlow carries more flow when no faults occur and suffers about the same amount of total loss during failures.

We have open-sourced an anonymous version of NCFlow [2], and are in the early stages of integrating NCFlow into production use at a large enterprise.

2 Background and Motivation

We analyze the changes in topology and traffic on a large enterprise WAN over a several-month period. As Figure 4

[1] short for **N**etwork **C**ontractions for **Flow** problems

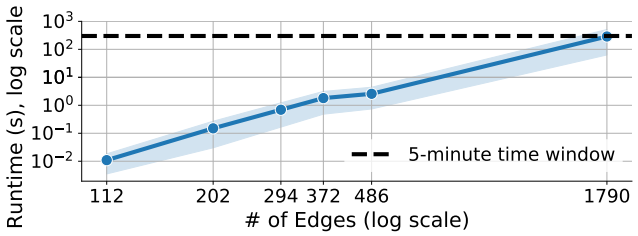

Figure 5: Runtimes of a state-of-the-art solver on topologies from Internet Topology Zoo [6]. Both axes are in log scale and the band represents standard deviation. In production WANs, new traffic demands arrive every few minutes [35, 38].

shows, the change in traffic demand from one 5-minute window to the next is substantial; the average change is 35%; in 20% of the cases, the traffic change is over 45%. The enterprise solves a global flow allocation problem every few minutes. The figure on the right shows the fraction of traffic that will remain unsatisfied if the flow allocation from the previous window were to be used instead of computing a new allocation. We see that the median loss is 13%; in 20% of the cases, over 20% of the demand remains unsatisfied. We verify that computing a new allocation will satisfy all of the demand; using the previous window's allocation causes loss because some datacenter pairs may receive more flow in the previous allocation than their current demand while other datacenter pairs go unsatisfied.

Given the above data, computing a new allocation in each time window is needed to carry more traffic on the WAN. However, solver runtime increases super-linearly with the size of the topology, as shown in Figure 5. For several public topologies and on a variety of traffic matrices, we benchmark the multi-commodity max-flow problem (specifically PF_4, as will be described in §5.1). The runtimes were measured on a server-grade machine using a production-grade optimization library [33]. As the figure shows, when the topology size exceeds a thousand edges, the time to compute a flow allocation can exceed the allotted time window.

A fast solver would not only ensure that new allocations complete in time—it could also enable more frequent allocations, e.g., every minute. Doing so would enable allocations to track changing demands at a finer granularity. Moreover, as we show in §5, a fast solver can help when reacting to link and switch failures.

Our observation that demand and capacity are concentrated among *nearby* nodes is grounded on the following measurements from a production WAN:

Demand properties:

- On average, 7% (or 16%) of the node pairs account for half (or 75%) of the total demand.
- When nodes are divided into a few tens of clusters, 47% of the total traffic stays within clusters. If the demands were distributed uniformly across node pairs, only 8% of the traffic would stay within clusters; thus the demand within clusters is about 6× larger than would be expected from a uniform distribution.

WAN topology properties:

- When nodes are divided into tens of clusters, 76% of all edges and 87% of total capacity is within clusters.
- The skew in capacity is small: the ratio between the largest edge capacity and the mean is 10.4.
- The skew in node degree is also small: the average node degree is 3.9, with $\sigma = 2.6$; the max is 16.
- Relative to the network size (hundreds of nodes), the average network diameter (=11) and the average shortest-path length (= 5.3) are very small.

Motivated by the above analyses, NCFlow seeks to be a fast solver for large WAN topologies by leveraging the concentration of traffic demands and capacity.

Background: Before we describe NCFlow's design, we give some background on multi-commodity flow problems. Given a set of nodes, capacitated edges, and demands between nodes, a flow allocation is feasible if it satisfies demand and capacity constraints. The goal of a multi-commodity flow problem is to find a feasible flow which optimizes a given objective; Table 1 lists some common flavors.

The fastest algorithms [27, 41] are approximate; i.e., given a parameter ε, they achieve at least $(1-\varepsilon)\times$ the optimal value. And, their runtime complexity is at least quadratic (Table 1).

Moreover, these solutions allow demands to travel on any edge, thus requiring millions of forwarding table entries at each switch for thousand-node topologies. Instead, production systems [35, 38] restrict flow to a small number of preconfigured paths per demand, which reduces the required forwarding table entries by 10–100×.

Using notation from Table 2, the feasible flow over a preconfigured set of paths can be defined as:

$$\begin{aligned}
\mathsf{FeasibleFlow}(\mathcal{V},\mathcal{E},\mathcal{D},\mathcal{P}) \triangleq \{ f_k \mid \forall k \in \mathcal{D} \text{ and } & \quad (1)\\
f_k = \sum_{p \in \mathcal{P}_k} f_k^p, \quad & \forall k \in \mathcal{D} \quad \text{(flow for demand } k\text{)}\\
f_k \le d_k, \quad & \forall k \in \mathcal{D} \quad \text{(flow below volume)}\\
\sum_{\forall k, p \in \mathcal{P}_k, e \in p} f_k^p \le c_e, \quad & \forall e \in \mathcal{E} \quad \text{(flow below capacity)}\\
f_k^p \ge 0 \quad & \forall p \in \mathcal{P}, k \in \mathcal{D} \quad \text{(non-negative flow)} \ \}
\end{aligned}$$

Production systems use linear optimization-based solvers [35, 36, 38]. On WANs with thousands of nodes, the optimization problem could have millions of variables and equations just to verify that a flow allocation is feasible.

In this paper, we consider the problem of maximizing the total flow across all demands:

$$\begin{aligned}
\mathsf{MaxFlow}(\mathcal{V},\mathcal{E},\mathcal{D},\mathcal{P}) \triangleq & \arg\max_{\mathbf{f}} \sum_{k \in \mathcal{D}} f_k \quad (2)\\
& \text{s.t.} \quad \mathbf{f} \in \mathsf{FeasibleFlow}(\mathcal{V},\mathcal{E},\mathcal{D},\mathcal{P})
\end{aligned}$$

	Maximization term	Additional Constraints	Used in	Known best complexity
MaxFlow	$\sum_{k\in\mathcal{D}} f_k$	none	[35, 38]	$O(M^2\varepsilon^{-2}\log^{O(1)}M)$ [27]
MaxFlow with Cost Budget	$\sum_{k\in\mathcal{D}} f_k$	$\sum_k \sum_{p\in\mathcal{P}_k} \sum_{e\in p} f_k^p \mathsf{Cost}_e \leq \mathsf{Budget}$		$O(\varepsilon^{-2}M\log M(M+N\log N)\log^{O(1)}M)$ [27]
Max Concurrent Flow	α	$d_k\alpha \leq f_k, \forall k \in \mathcal{D}$	[19, 39, 40]	$O(\varepsilon^{-2}(M^2+KN)\log^{O(1)}M)$ [41]

Table 1: We illustrate a few different multi-commodity flow problems all of which find feasible flows but optimize for different objectives and can have additional constraints; see notation in Table 2. Equation 6 fleshes out the problem completely for the case of maximizing flow. More problems are discussed in [11].

Term	Meaning
$\mathcal{V}, \mathcal{E}, \mathcal{D}, \mathcal{P}$	Sets of nodes, edges, demands, and paths
N, M, K	The numbers of nodes, edges, and demands, i.e., $N = \lvert\mathcal{V}\rvert, M = \lvert\mathcal{E}\rvert, K = \lvert\mathcal{D}\rvert$
e, c_e, p	Edge e has capacity c_e; path p is a set of connected edges
(s_k, t_k, d_k)	Each demand k in $\mathcal{D}$ has source and target nodes ($s_k, t_k \in \mathcal{V}$) and a non-negative volume (d_k).
$\mathbf{f}, f_k^p$	Flow assignment vector for a set of demands and the flow for demand k on path p.

Table 2: Notation for framing multi-commodity flow problems.

$\mathcal{V}_{\text{agg}}$, $\mathcal{E}_{\text{agg}}$, $\mathcal{D}_{\text{agg}}$, $\mathcal{P}_{\text{agg}}$	Nodes, edges, demands, and paths in the aggregated graph
$\mathcal{V}_x, \mathcal{E}_x, \mathcal{D}_x, \mathcal{P}_x$	Subscript denotes entities in the restricted graph for cluster x
x, η	Each cluster x is a strongly connected set of nodes and η is the number of clusters
$k, K_{xy}, K_{sy}, K_{xt}$	An actual demand (k); the rest are bundled demands from one source (s) or all nodes in a cluster (x) to a target (t) or to all nodes in a cluster (y)

Table 3: Additional notation specific to NCFlow.

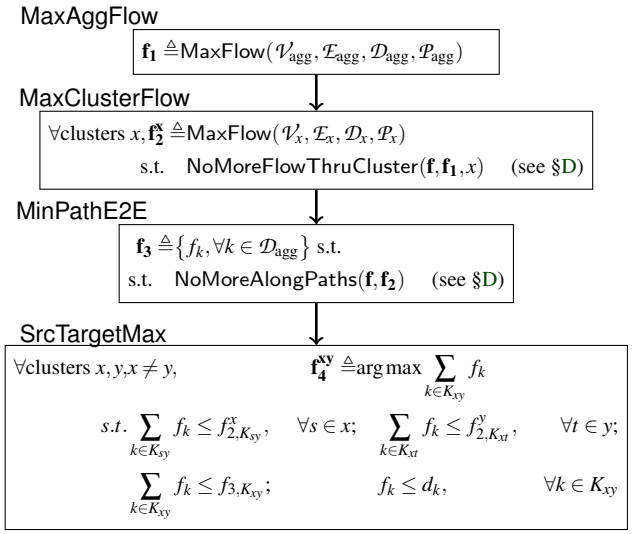

Figure 6: The basic flow allocation algorithm used by NCFlow; notation used here is defined in Table 3.

SDN-based traffic engineering schemes [35, 38], in addition to repeatedly solving global optimizations, must maintain an up-to-date view of the topology, gather desired volumes for demands and update traffic splits at switches based on the result of the optimization. Our production experience is that most of these repetitive steps have a latency of a few RTTs (round trip times) and so solving the optimization dominates, especially on large topologies. Moreover, demands are limited to their allocated rates in software at the source servers and thus allocating less than the full desired rate need not result in packet loss [35]. Finally, applications that contribute a large fraction of the bytes moving between datacenters are elastic in short timescales; e.g., large dataset transfers for data analytics. That is, these apps seek a fast completion time but do not need a large rate in every optimization epoch. Some other applications have a decreasing marginal utility as their rate allocation increases such as video streams of varying quality [43]. Today's SDN-based TE solutions [35, 38] use multiple priority classes to maximize allocations for elastic traffic without affecting the latency-sensitive traffic.

3 NCFlow

In this section, we describe NCFlow. Our steps are as shown in Figure 1. Offline, based on historical demands, we divide the network into clusters and determine paths. Further details are in §3.4. Online, we allocate flow to the current demands by solving a carefully constructed set of simpler sub-problems, some of which can be solved independently and in parallel. We describe these sub-problems in §3.1. Although they can be solved quickly, disagreements between independent solutions can lead to infeasible allocations; we present a simple heuristic in §3.2 that provably leads to feasible flow allocations. In §3.3, we discuss extensions that increase the total flow allocated by NCFlow. We also show sufficient conditions under which NCFlow is optimal and matches the flow allocated by MaxFlow. Finally, in §3.5, we discuss how NCFlow uses fewer forwarding entries by reusing pathlets within clusters and splitting rules for different demands.

3.1 Basic Flow Allocation

We begin by describing a simple (but incomplete) version of NCFlow's flow allocation algorithm; the pseudocode is in Figure 6. We continue using Figure 2 as a running example. The basic algorithm proceeds in four steps.

In the first step, we allocate flow on the aggregated graph; as shown in MaxAggFlow in Figure 6. In the aggregated graph, an example of which is in Figure 2 (right), nodes are clusters and the edges are bundled edges from the original graph—the edge between the red and yellow clusters corresponds to the five edges between these clusters on the actual graph. Similarly, we bundle demands on the aggregated graph: the demand K_{xy} between the clusters x and y corresponds to all of the demands whose sources are in cluster x and targets are

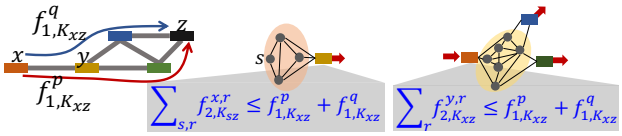

Figure 7: An example illustrating how the flow allocated in MaxAggFlow translates to constraints on the flow to be allocated in MaxClusterFlow.

in cluster y. The resulting flow allocation ($\mathbf{f_1}$) accounts for bottlenecks on the edges between clusters. However, this flow may not be feasible, since there may be bottlenecks *within* the clusters.

In the second step, we refine the allocation from step 1 to account for intra-cluster demands and constraints. Specifically, we allocate flow for the demands whose sources and targets are within the cluster. We also allocate no more flow than was allocated in $\mathbf{f_1}$ for the inter-cluster flows. MaxClusterFlow in Figure 6 shows code for this step. We note a few details:

- We use virtual nodes to act as the sources and targets for the inter-cluster flows; the flow allocated in $\mathbf{f_1}$ determines which virtual node (i.e., which neighboring cluster) is the sender or the receiver for an inter-cluster demand.
- Figure 7 shows two examples on the right where the virtual nodes are drawn using squares.
- Figure 7 also shows the NoMoreFlowThruCluster constraints for demands from sources in the red cluster to targets in the black cluster (depicted as x and z respectively). On the aggregated graph, the flow for this demand takes the two paths shown. In the red cluster, as shown in the equation, the traffic from all sources (s), along multiple paths (r) to the virtual node, is restricted to be no more than what was allocated in $\mathbf{f_1}$.
- Figure 7 on the right also shows a more complex case that happens in the yellow cluster. Here, the traffic arrives at one virtual node but can leave to multiple virtual nodes. In MaxClusterFlow, we set up paths between all pairs of virtual nodes. As shown in the equation, the traffic leaving the red virtual node on paths (r) to either of the other virtual nodes must be no more than the total flow on paths p and q from $\mathbf{f_1}$.
- Observe that bundling demands ensures fewer variables and constraints for MaxClusterFlow. The demand from red to black clusters comprises twenty node pairs in the actual graph in Figure 2 (left); four sources in the red cluster and five targets in the black cluster. However, the MaxClusterFlow for the red cluster only has four bundled demands, from each source to the virtual node, and the yellow cluster has just one bundled demand from and to virtual nodes.

In the third step, we reconcile end-to-end; that is, we find the largest flow that can be carried along each path on the aggregate graph. As shown by MinPathE2E in Figure 6, for each bundle of demands and each path, we take the minimum flow allocated ($\mathbf{f^x_2}$) at each cluster on the path.

The flow allocation for the demands in a cluster x can be read directly from the $\mathbf{f^x_2}$ solution of MaxClusterFlow. For demands that span clusters, however, more work remains because the steps thus far do not directly compute their flow. In particular, $\mathbf{f_3}$ allocates flow for cluster bundles; such as say for all the demands whose sources are in cluster x and targets are in cluster y. The corresponding per-cluster flow allocations, $\mathbf{f^x_2}$ and $\mathbf{f^y_2}$, allocate flow from a source node and to a given target respectively. Thus, in the final step, SrcTargetMax, we assign the maximal flow to each inter-cluster demand that respects all previous allocations.

Problem	# of Nodes	# of Edges	# of Demands
MaxFlow	N	M	K
MaxAggFlow	η	$\le \min(M, \eta^2)$	$\le \min(K, \eta^2)$
MaxClusterFlow	$\sim \frac{N}{\eta} + \eta$	$\sim \frac{M}{\eta} + 2\eta$	$\sim \frac{K}{\eta^2} + 2\frac{N}{\eta} + \eta^2$

Table 4: Sizes of the problems in Figure 6 using notation from Tables 2 and 3. Just verifying that flow is feasible (i.e., FeasibleFlow in Eq. 1) uses $O(\#\text{ nodes} * \#\text{ edges})$ number of equations and variables. NCFlow has one instance of MaxAggFlow and executes the η instances of MaxClusterFlow in parallel. MinPathE2E and SrcTargetMax, are relatively insignificant.

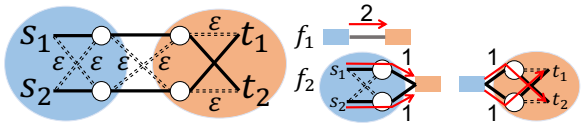

(a) Disagreement arising from bundling edges: As shown on the right, the algorithm in Figure 6 will allocate 2 units of flow but only 5ε units can be carried.

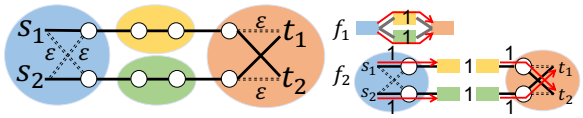

(b) Disagreement arising from bundling demands: As shown on the right, the algorithm in Figure 6 will allocate 2 units of flow, but only 2ε units can be carried.

Figure 8: Illustrating how disagreements in flow allocation can occur in the basic flow allocation algorithm; see §3.1.1.

3.1.1 Properties of Basic Flow Allocation

Solver runtime: The numbers of equations and variables in the sub-problems are shown in Table 4. If the number of clusters η is 1, note that there is exactly one per-cluster problem, MaxClusterFlow, which matches the original problem from Eqn. 2. When using a few tens of clusters, we will show in §5 that all of the sub-problems are substantially smaller than the original problem (MaxFlow).

Feasibility: The flow allocated by Figure 6 satisfies demand and capacity constraints; we will prove this formally in §B.1. For demands whose source and target are in different clusters, however, disagreements may ensue since the different problem instances assign flow to different bundles of edges and demands. We illustrate two such examples in Figure 8; both have 1 unit of demand from s_1 to t_1 and from s_2 to t_2. The dashed edges have a capacity of $\varepsilon \ll 1$ and all of the other edges have a very large capacity.

- The example in Figure 8a illustrates an issue with bundling edges. The actual graph on the left can only

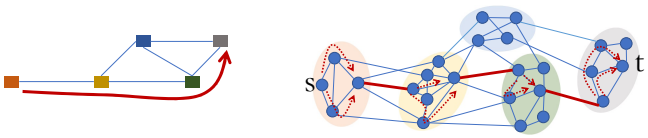

Figure 9: To guarantee feasibility, each cluster bundle is allocated flow on only one path on the aggregated graph (left) and on only one edge between each pair of clusters (right); the usable path and edges are shown in dark red. Note that multiple paths can still be used within clusters.

carry 5ε units of flow for each demand. However, as the figures on the right show, MaxAggFlow allocates two units of flow since the four edges between these two clusters can together carry all of the two units of demand. The MaxClusterFlow instances also allocate two units of flow as shown. The discrepancy arises because the problems in Figure 6 do not know that the *top* egress of the left cluster can take in all of the demand of s_1 but has only a low capacity to t_1.

- The example in Figure 8b illustrates an issue with bundling demands. Here too, observing the actual network on the left will show that 2ε units can be carried for each demand split evenly between the top and the bottom path. Again, as the figures on the right show, the basic flow allocation algorithm will conclude that both units of demand can be carried. Here, the discrepancy arises from the bundling of demands, the problems in Figure 6 cannot discern that the MaxClusterFlow instance of the left cluster sends the first demand to the brown cluster while the MaxClusterFlow of the right cluster wants to receive the second demand from the brown cluster.

3.2 A feasible heuristic

To avoid end-to-end disagreements, we make two simple changes to the basic flow allocation in §3.1.

First, when solving MaxAggFlow, only one path on the aggregated graph can be used for all of the demands between a given pair of clusters; we call such groups of demands to be cluster bundles. Next, between a pair of connected clusters, only one edge can carry the flow for a cluster bundle. Figure 9 shows in dark red an example path for a cluster bundle and the allowed edges between clusters; we also show the intra-cluster paths that can carry flow for this bundle.

There are multiple ways to avoid disagreements while keeping the problem sizes small via bundling. We discuss the above changes here because they are simple and sufficient. Specifically, we show that:

Theorem 1. *The algorithm in Figure 6, when constrained as discussed above, will always output a feasible flow.*

Proof. The proof is in §B.2. Intuitively, these changes suffice because the independent decisions made by different problems in Figure 6 cannot disagree; per cluster bundle, all problem instances allocate flow to the same edge and path. □

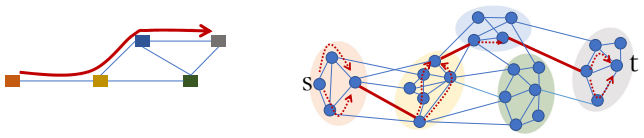

Figure 10: Contrasting with Figure 9, for the same cluster bundle, in a subsequent iteration, NCFlow allocates flow on a different path on the aggregate graph and on different inter-cluster edges. The chosen paths and edges are again shown in red.

3.3 Stepping towards optimality

The flow allocation algorithm described thus far is fast but not optimal; that is, it may allocate less total flow over all demands than the flow allocated by solving the larger global problem (MaxFlow from Eqn. 2). There are a few reasons why this happens. The MaxAggFlow in Figure 6 allocates flow on paths through clusters without knowing how much flow the clusters can carry. Switching the order, i.e., solving MaxClusterFlow before MaxAggFlow, could be worse because each cluster must allocate flow without knowing how much flow can be carried end-to-end. Furthermore, the heuristic in §3.2 constrains each cluster bundle to use only one edge between clusters and one path on the aggregated graph. We now discuss a few extensions to increase the flow allocation.

First, we re-solve the problems in Figure 6 multiple times. A simple way to do this would be to deduct the allocated flow and use the residual capacity on edges in the next iteration. Also, we pick different edges between clusters and/or different paths on the aggregated graph in different iterations (see Figure 10 for an example). The number of iterations is configurable; we continue as long as the total flow increases in each iteration by at least a pre-specified amount (say 5%). One could apply other policies such as a timeout. We show in §5 that a small number of iterations suffice for a sizable increase in the total flow. We will also show that later iterations finish faster than the first iteration perhaps because fewer demands remain to satisfy.

Next, we empirically observe that the choice of clusters and edges/paths to use in different iterations has an effect on flow allocation. For instance, the disagreements in Figure 8 *go away* by using a different choice of clusters—specifically, see Figure 31d and Figure 31e. We discuss how NCFlow precomputes cluster and edge/path choice in §3.4.

To sum up, we prove that flow allocation will be optimal when a few sufficient conditions hold:

Theorem 2. *The method in Figure 6 leads to the optimal flow allocation when any path can be used within each optimization and the number of clusters is* 1 *or equal to the number of nodes or all of the following conditions hold:*

- *the aggregated graph $\mathcal{G}_{agg}$ is a tree,*
- *only one edge connects any pair of clusters,*
- *all demands are satisfiable.*

Proof. By optimal, we mean that the total allocated flow must be as large as an instance of Equation 6 wherein any path can be used. The proof is in §B.3. Intuitively, when the number of clusters is 1 and any paths can be used, a single instance of MaxClusterFlow is identical to the optimal problem in Equation 6. Similarly, when the number of clusters equals the number of nodes, MaxAggFlow is identical to the optimal problem. Furthermore, the conditions listed lead to optimality because the optimal flow allocation can be transformed into an allocation that can be outputted by Figure 6. □

Even though the listed conditions appear restrictive, note that the topology within clusters can be arbitrary. We will show in §5 that NCFlow offers nearly optimal flow allocations even when the above conditions do not hold.

3.4 Choosing clusters and paths

The choice of clusters and paths affects both the solution quality and runtime of NCFlow. We cast cluster choice as a graph partitioning problem [5, 21, 65] with these objectives:

- **Concentrated with a low cut:** NCFlow can output better flow allocations when much of the total demand and the total edge capacity is between nodes in the same cluster.
- **Balanced cut:** Intuitively, NCFlow will have a smaller runtime when the complexity of MaxAggFlow balances with that of MaxClusterFlow. Recall from Table 4 that the former depends on the number of clusters whereas the latter depends on the size of the largest cluster.

We empirically observe, based on experiments with many WANs and different types of demands, that:

- On a graph with N nodes, about $\sqrt{N}$ clusters, irrespective of the clustering technique, leads to the best result, i.e., smallest runtime and fewest forwarding entries while allocating nearly the largest amount of flow possible; see Figure 13.
- When choosing the same number of clusters, one of the three considered clustering techniques (described below) generally performs better than the others but not in all cases; see Figure 21.

Thus, the *optimal* clustering choice for a WAN is unclear; it is possible that hand-tuning or using a learning technique may lead to better-performing clusters. Nevertheless, any of the three simple clustering schemes discussed below already suffice for NCFlow to improve substantially over baselines.

We consider the following clustering choices because they are simple and fast; unless otherwise noted, results in this paper use FMPartitioning.

- FMPartitioning [18, 25] divides nodes into clusters so as to maximize a "modularity" score which prefers more edges to lie within than between clusters. In NCFlow, we apply modularity-based clustering with edge weights set to their capacity.
- Spectral clustering [53] computes eigenvectors of the weighted adjacency matrix and chooses a desired number of the top eigenvectors as *cluster heads*; each node is assigned to the cluster of their closest eigenvector (e.g., using k-means).
- Leader Election picks a desired number of nodes at random as leaders and assigns each other node to the closest leader; wherein, distance is measured as the path length using invcap edge weights.

Some other clustering techniques [5, 42, 65] can balance cluster sizes or trade-off between concentration and balance but are more complex computationally; it is possible that using such schemes can further improve NCFlow.

Path choice in NCFlow: On the aggregated graph and on each cluster graph, we pre-compute offline a small number of paths between every pair of nodes. We consider the following different path choices and pick paths that lead to the largest flow allocation on historical demands:

- k-shortest paths [70] with edge weight of 1 or $\frac{1}{c_e}$ where c_e is the capacity of edge e and $k = 4, 8$ or 16.
- As above, but with the additional requirement that the paths for a node pair are edge-disjoint [52].

NCFlow also pre-computes offline (1) a pseudo-random choice of which edges to use between a pair of connected clusters in each iteration and (2) which path on the aggregated graph to use for each cluster bundled demand in each iteration.

3.5 Setting up switch forwarding entries

NCFlow uses many fewer switch forwarding entries than prior works due to the following reasons.

First, the paths along which NCFlow allocates flow can be thought of as a sequence of pathlets [32, 47, 68] in each cluster connected by crossing edges between clusters. Figures 9 and 10 illustrate such paths on the right. This observation is crucial because a pathlet can be reused by multiple demands. For example, in Figure 9, the flow from any source in the red cluster to any target in the grey cluster would use the same pathlets shown in the yellow, green, and blue clusters. Prior work [35, 36], on the other hand, establishes paths for each demand. Using pathlets has two advantages. The number of pathlets used by NCFlow is about η times less than the number of paths used by prior works[2]. Furthermore, a typical pathlet has fewer hops than a typical end-to-end path. Thus, NCFlow uses many fewer rules to encode paths in switches.

[2]More precisely, the number reduces from $PN(N-1)$ to $\sum_x P(N_x)(N_x-1)$ where P is the number of paths per node pair, the N nodes are divided into η clusters, and cluster x has N_x nodes. If clusters are evenly sized, $N_x = N/\eta$, and the ratio of these terms is $\sim \eta$.

Next, whenever NCFlow allocates flow at the granularity of cluster bundles, all of the demands in a bundle take the same paths and are split in the same way across paths. Hence, NCFlow uses one traffic splitting rule for all demands in such bundles. For instance, the demands from source s in the red cluster in Figure 9 to any target in the grey cluster are split with the same ratio across the same pathlets in all clusters (except the grey cluster where they take different pathlets to reach their different targets). Thus, with NCFlow, the number of splitting rules at a source decreases by a factor of $\sqrt{N}/2$[3].

The paths and splitting rules to push into switch forwarding tables are determined by the offline component of NCFlow and only change occasionally. After each allocation, only the splitting ratios change. More details on the data-plane of NCFlow such as how to compute the total flow that can be sent by each demand and the splitting ratios as well as how to move packets from one pathlet to the next are in Appendix C. In §5, we measure the numbers of rules used by NCFlow.

4 Implementing NCFlow

Our current prototype of NCFlow is about 5K lines of Python code, which invokes Gurobi [33] v8.1.1 to solve all of the optimization problems. For clustering WAN topologies, we adapt [26] to find clusters that maximize modularity; we also use our own implementation of NJW spectral clustering [53]. We use a grid search over the number of clusters (η) and the above clustering techniques to identify the best performing choice for each topology on a set of historical traffic matrices. To compare with state-of-the-art techniques, we customize the public implementations of SMORE [44, 45] and TEAVAR [19]. We have also implemented Fleischer's algorithm [27]; our implementation is about 10× faster than public implementations [8, 37] since we carefully optimize a key bottleneck in Fleischer's algorithm. All of these code artefacts are available on GitHub [2].

5 Evaluation

We evaluate NCFlow on several WAN topologies, traffic matrices, and failure scenarios to answer the following questions:

- Compared to state-of-the-art LP solvers and approximate combinatorial algorithms, does NCFlow offer a good trade-off between runtime and total flow allocation? Is it substantially faster, with only a small decrease in total flow?
- For real-world TE scenarios, in which flow solvers must adapt to changing demands and faults, how much benefit does NCFlow offer relative to the state-of-art?

[3] A source uses $N-1$ splitting rules in prior works but with NCFlow only requires $N_x+\eta-2$ rules when the source's cluster has N_x nodes; if clusters are evenly sized and $\eta \sim \sqrt{N}$, the ratio of these terms is $\sqrt{N}/2$.

Topology	# Nodes	# Edges	# Clusters
PrivateLarge	∼ 1000s	∼ 1000s	31
Kdl	754	1790	81
PrivateSmall	∼ 100s	∼ 1000s	42
Cogentco	197	486	42
UsCarrier	158	378	36
Colt	153	354	36
GtsCe	149	386	36
TataNld	145	372	36
DialtelecomCz	138	302	33
Ion	125	292	33
Deltacom	113	322	30
Interoute	110	294	20
Uninett2010	74	202	24

Table 5: Some of the WAN topologies used in our evaluation; see §5.1.

- How do our various design choices in NCFlow impact its performance?

5.1 Methodology

Here, we describe our methodology—the topologies, traffic, baselines, and metrics used in our evaluation.

Topologies: We use two real topologies from a large enterprise—PrivateSmall is a production internet-facing WAN with hundreds of sites, and PrivateLarge is a larger WAN that contains many more sites. We also use several topologies from the Internet Topology Zoo [6] and reuse topologies used by prior works [19, 38]. Table 5 shows details for some of the used topologies; note that the topologies shown are 10× to 100× larger than those considered by prior work [19, 35, 38, 44, 49].

Traffic Matrices (TMs): We benchmark NCFlow on traffic traces from PrivateSmall, which contain the total traffic between node pairs at 5-minute intervals. We also generate the following kinds of synthetic traffic matrices for all topologies:

- **Poisson**(λ, δ) models demands with varying concentration; the demand between nodes s and t is a Poisson random variable with mean $\lambda\delta^{d_{st}}$, where d_{st} is the hop length of the shortest path between s and t and $\delta \in [0,1)$ is a *decay factor*. We choose δ close to 0 or to 1 to model strongly and weakly concentrated demands, respectively.
- **Gravity**(v) [14, 60]: The total traffic leaving a node is proportional to the total capacity on the node's outgoing links (parameterized by v); this traffic is divided among other nodes proportional to the total capacity on their incoming links.
- **Uniform**$([0,a))$: The traffic between any pair of nodes is chosen uniformly at random, between 0 and a.
- **Bimodal**$([0,a),[b,c),p)$ [14]: A p fraction of the node pairs, chosen uniformly at random, receive demands from **Uniform**$([b,c))$ while the rest receive demands from **Uniform**$([0,a))$. We use $p = 0.2$.

For each above model, we select parameters such that fully satisfying the traffic matrix leads to a maximum link utiliza-

tion of about 10% in each topology. Then, we scale all entries in the TM by a constant $\alpha \in \{1,2,4,8,16,32,64,128\}$. Doing so creates demands that range from easily satisfiable to only partially satisfiable; with $\alpha = 128$, the satisfiable portion of the demand varies between 25-70%. We generate five samples for each traffic model and scale factor for each topology.

Baselines: We compare NCFlow with these techniques:

Path Formulation (PF_4) solves the multi-commodity max-flow problem shown in Equation 2 using k-shortest paths between node pairs where $k = 4$. Results for other path choices are in §G.4.

PF *Warm Start* (PF_{4w}) matches PF_4 except that it allows the LP solver to "warm start"; that is, over a sequence of traffic matrices, the flow allocated to the previous TM is used as a starting point to compute allocation for the next TM. When traffic changes are small, warm start leads to faster solutions.

Approximate Combinatorial Algorithms: Fleischer's algorithm [27] is the best-known approximation for MaxFlow. We use two variants: Fleischer-Path where flow is restricted to a path set and Fleischer-Edge without any path restrictions. We show results here for an approximation guarantee of 0.5; that is, the techniques must achieve at least half of the optimal flow allocation. Results for other approximation guarantee values are in [10].

SMORE [44] allocates flow dynamically on paths that are pre-computed using Räcke's Randomized Routing Trees (RRTs). We use the code from [45] to compute paths. Since the LP in [45] requires demands to be fully satisfiable, we implement a variant, SMORE*, that maximizes the total flow on the computed paths, regardless of demand satisfiability.

TEAVAR [3,19] models link failure probabilities and computes flow allocations given an availability target. We implement a variant, TEAVAR*, that maximizes the total flow[4]; further details are in Appendix F.

Clusters, Paths, and # of Iterations: Table 5 shows the number of clusters used by NCFlow per topology. Here, we report results on edge-disjoint paths, chosen using inverse capacity as the edge length; results for other path choices are qualitatively similar (see §G.4). All schemes that use paths (i.e., PF_4, Fleischer-Path, TEAVAR*, and NCFlow) use the same method to compute paths. For each iteration up to $I = 6$, we also pre-compute offline the path to use on the aggregated graph, and the edge to use between connected clusters for each cluster bundle.

Metrics: We compare the schemes on the following metrics:

- **Relative total flow** is the total flow achieved by a scheme relative to PF_4.
- **Speedup ratio** is the runtime of each scheme relative to PF_4. For LP-based methods, we report the Gurobi solver runtimes, since models can be constructed once offline in practice. For combinatorial methods, we report algorithm execution time. All runtimes are measured on an Intel Xeon 2.3GHz CPU (E52673v4) with 16 cores and 112 GB of RAM.
- **FIB Entries:** We measure the number of switch forwarding entries used.

[4]TEAVAR [3, 19] maximizes the *concurrent* flow; see Table 1

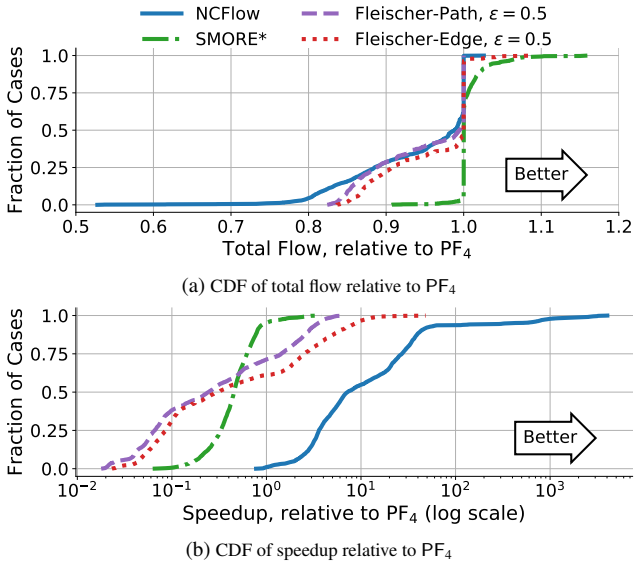

(a) CDF of total flow relative to PF_4

(b) CDF of speedup relative to PF_4

Figure 11: CDFs comparing NCFlow with state-of-the-art methods. With only a modest decrease in total flow, NCFlow offers a substantial runtime speedup.

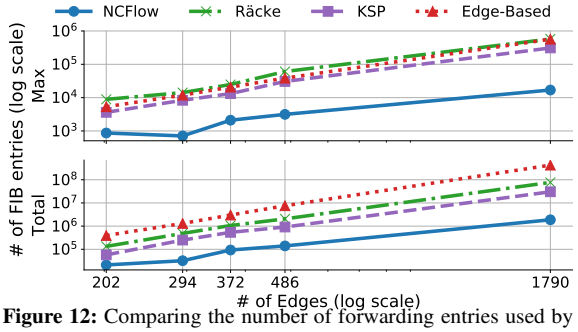

Figure 12: Comparing the number of forwarding entries used by various methods for the experiments from Figure 11.

5.2 Comparing NCFlow to the State of the Art

Figures 11a and 11b show cumulative density functions (CDFs) of the relative total flow and speedup ratio for NCFlow and several baselines. These results consist of 2,600 traffic matrices and 13 topologies. If a scheme matches the baseline PF_4, its CDF will be a pulse at $x = 1$ in both figures; the fraction of cases to the left (or right) of $x = 1$ indicate how often a scheme is worse (or better) than PF_4. Note that the x-axis for the speedup ratio is in log scale.

We see that SMORE*, shown using green dashed lines in the figures, modestly improves the flow allocation (in 25% of the cases) while almost always taking longer to run than PF_4.

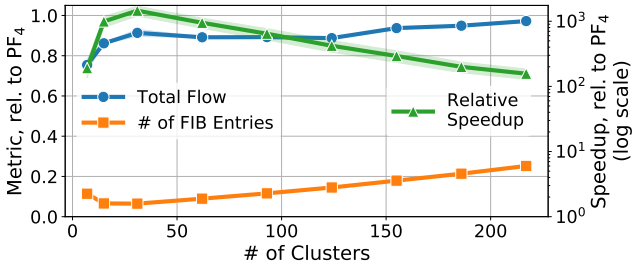

Figure 13: NCFlow's performance when using different numbers of clusters on PrivateLarge. The speedup ratio is plotted on the right y-axis in log scale; the other metrics use the left y-axis.

Both effects are because SMORE* allocates flow on Räcke's RRTs instead of k-shortest paths.

The edge and path variants of Fleischer's, shown using purple and red lines in the figures, perform similarly; since they are approximate algorithms, they allocate less flow than PF_4 in roughly 50% of cases, but are also faster than PF_4 in slightly less than 50% of cases. We conclude that these approximate algorithms are not practically better than PF_4.

In contrast, NCFlow, shown with dark blue lines in the figures, almost always allocates at least 80% of PF_4's total flow, while achieving large speedups. In the median case, NCFlow achieves 98% of the flow and is over 8× faster. These improvements accrue from NCFlow solving smaller optimization problems than PF_4.

Figures 18 and 19 tease apart the above results by load, traffic type and topology. Figures 23–27 show results for alternate path choices. Taken together, these results indicate that NCFlow's improvements hold across a variety of scenarios.

For the same experiments considered above, Figure 12 shows the number of switch forwarding entries used in different topologies. (A full set of results is in Table 6.) The bottom plot is the total number of forwarding entries across all switches, while the top shows the maximum for any switch. Note that both the x and y axes are in log scale. NCFlow consistently uses fewer forwarding entries; using NCFlow offers a greater amount of relative savings than switching from all edges to just a handful of paths per demand. The savings from NCFlow also increase with topology size. The reason, as noted in §3.5, is that NCFlow reuses pathlets and traffic splitting rules for many different demands.

5.3 Effect of Design Choices

Figure 13 shows how NCFlow's performance varies with the numbers of clusters used on PrivateLarge. While NCFlow allocates roughly the same amount of total flow, using about 30 clusters improves runtime and reduces forwarding entries. Figure 21 compares NCFlow's performance when using different clustering techniques; more details are in §G.2.

Recall from §3.3 that NCFlow uses multiple iterations of Figure 6. In the above experiments, the first iteration alone accounts for 75% of the runtime and for roughly 90% of the flow that is allocated by NCFlow. Later iterations are faster perhaps because they have less traffic to consider.

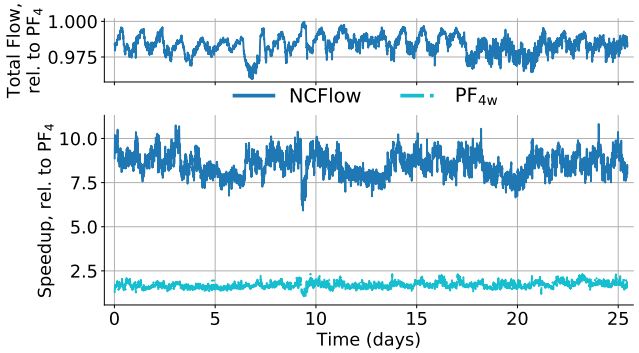

Figure 14: Allocated flow and speedup relative to PF_4 on a sequence of production TMs from PrivateSmall. In half of the cases, NCFlow allocates at least 98.5% of the flow and is at least 8.5× faster.

Breaking down the runtime by the steps in Figure 6, we see cases where MaxClusterFlow accounts for over 70% of NCFlow's runtime perhaps because the largest cluster contains a large fraction of the nodes. Better cluster choice or recursively dividing the largest clusters can further lower runtime.

5.4 NCFlow on Real-World Traffic

Here, we experiment with a sequence of traffic traces collected on the PrivateSmall WAN. Figure 14 plots the moving average (over 5 windows) of the total flow and speedup relative to PF_4 for two schemes—NCFlow in blue and PF_{4w} in light blue. The figure shows that PF_{4w}'s warm start yields a median speedup of 1.66×. NCFlow achieves a consistently higher speedup (8.5× in the median case), and the flow allocation is nearly optimal: the median total relative flow is 98.5%, and NCFlow always allocates more than 93%.

5.5 Tracking Changing Demands

Here, we evaluate the impact of a technique's runtime on its ability to stay on track with changing demands. Specifically, on the PrivateLarge topology, we use a time-series of traffic matrices, wherein a new TM arrives every five minutes and the change from one TM to the next is consistent with the findings in Figure 4 (more details are in Figure 20). At each time-step, all techniques have the opportunity to compute a new allocation for the current TM or to continue computing the allocation for an earlier TM if they have not yet finished; in the latter case, their most recently computed allocation will be used for the current TM. For example, a technique that requires five minutes to compute a new allocation will be always *one window behind*, i.e., each TM will receive the allocation that was computed for the previous TM.

Figure 15 shows the fraction of demand that is satisfied by three different schemes; we also show the value for an instantaneous scheme which is not penalized for its runtime.

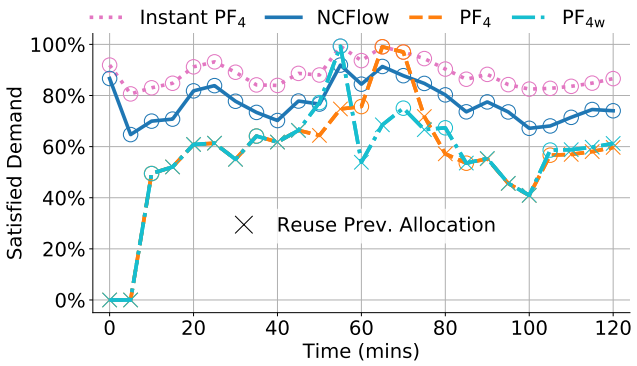

Figure 15: When demands change, how solver runtimes affect flow allocation on PrivateLarge: Due to the slow runtime, PF_4 and PF_{4w} carry only 62% of the traffic that can be satisfied by Instant PF_4, a (hypothetical) scheme which has zero runtime. NCFlow carries 87% of the traffic since its faster runtime compensates for its sub-optimality.

PF_4's average runtime here is over 15 minutes; hence, as the orange dashed line shows, PF_4 is able to compute a new allocation only for every third or fourth TM. This leads to substantial demand being unsatisfied: for node pairs whose current demand is larger than before, PF_4 will not allocate enough flow. On the other hand, node pairs whose current demand is less than their earlier demand will be unable to fully use PF_4's allocation. As the figure shows, PF_4 only satisfies 53% of the changing demand on average, whereas Instant PF_4 satisfies 87% of the demand.

PF_{4w} (the dash-dot light blue line), where the solver warm starts using the previous allocation, is modestly faster than PF_4 on average. As the figure shows, the average demand satisfied by PF_{4w} is only slightly larger than PF_4 (about 54%).

In contrast, NCFlow (the solid dark blue line) finishes well within five minutes which allows allocations to change along with the changing demands. We find that on average NCFlow satisfies 75% of the demands; its smaller runtime more than makes up for sub-optimality, allowing NCFlow to carry more flow than PF_4 when demands change.

5.6 Handling Failures with NCFlow

Here, we evaluate the effect of link failures. As we note in §F, TEAVAR* did not finish within several days on any of the topologies listed in Table 5 because when all possible 2-link failure scenarios are considered, the number of equations and variables in the optimization problem increase from $O(N^2)$ for MaxFlow to $O(M^2N^2)$ for TEAVAR [19], where N and M are the numbers of nodes and edges, respectively. Hence, we report results on the 12-node, 38-edge WAN topology from B4 [38]. We generate synthetic traffic matrices as noted in §5.1. Using link failure probabilities from TEAVAR [3], we generate several hundred failure scenarios and, for each TM, we measure the flow carried by NCFlow and TEAVAR* before the fault, immediately after the fault, and after recovery.

A key difference in fault recovery between NCFlow and TEAVAR* is that TEAVAR* requires sources to rebalance the

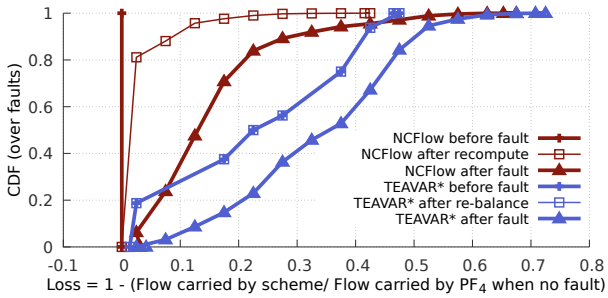

(a) CDFs of the flow *loss* before faults, immediately after faults and after recovery (B4 topology, many traffic matrices and faults; see §5.6).

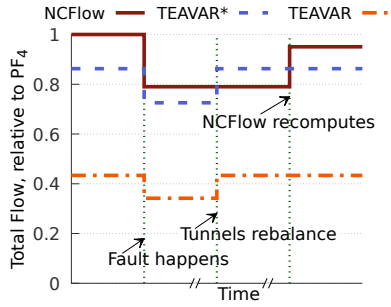

(b) Timelapse of when a fault occurs (B4 topology, Uniform traffic matrix, $\beta = 0.99$)

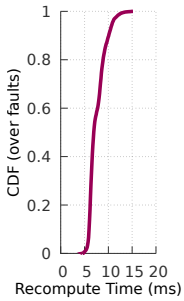

(c) NCFlow's time to recompute after fault.

Figure 16: Comparing failure response of NCFlow with prior work.

traffic splits when a failure happens; doing so takes about one RTT on the WAN. Given a parameter β, TEAVAR* guarantees that there will be no flow loss after the tunnels re-balance with a probability of $1-\beta$. See §F for more details. We use $\beta = 0.99$, as recommended in [19]. NCFlow, on the other hand, recomputes flow allocations taking into account the links that have failed; doing so takes one execution of NCFlow and some RTTs to change the traffic splits at switches; more details are in §E. Figure 16c shows that the recomputation time is well within one RTT on the WAN.

Figure 16b shows a timelapse of the flow carried on the network before the fault, immediately after the fault, and after recovery. As the figure shows, TEAVAR* can have a smaller loss and for a shorter duration; i.e., until sources rebalance traffic while NCFlow can carry more flow before fault and after recovery; moreover, the fast solver time can reduce the duration of loss.

Figure 16a shows CDFs over many faults and traffic matrices for NCFlow and TEAVAR*. We record the flow loss at three stages: before the fault, immediately after the fault, and after recovery. As the figure shows, NCFlow's ability to carry more flow before the fault and after recovery more than compensates for the slightly larger loss it may accrue in between.

6 Discussion

Extending beyond MaxFlow: FeasibleFlow is a common constraint for many objectives beyond MaxFlow (see Table 1). Since the algorithm in §3.1 and the heuristic in §3.2 guarantee feasibility, NCFlow can apply to objectives beyond MaxFlow;

however, we believe that more work is needed to improve the solution quality for different objectives.

Optimality guarantee: In §I, we show that constraining by clusters and paths, as done by NCFlow, does not necessarily reduce the flow allocation; that is, nearly the maximum amount of flow can be carried while respecting clustering and path constraints. This is promising because a better heuristic (than Figure 6) may allocate more flow without losing the benefits of solving smaller per-cluster problems. Furthermore, although NCFlow achieves sizable speedups by using simple clustering methods, the optimal cluster choice is uncertain; we show examples in §H to illustrate the challenges.

Recursive (or multiple levels of) clusters: For large topologies or when the largest cluster has a disproportionate number of nodes, we can further divide a cluster into sub-clusters. Doing so is an extension of the algorithm in Figure 6 where, in the iterative step, the MaxClusterFlow problem at a cluster is replaced with a new instance of all of the steps in Figure 6 along with the additional constraints that arise from the current level (e.g., NoMoreFlowThruCluster constraints). We leave further details to future work.

7 Related Work

NCFlow builds upon a few themes in prior work. We discuss and evaluate against some prior works already. To recap: (1) Some large enterprises use path-based global optimization problems similar to MaxFlow to manage traffic on their WANs [35, 36, 38]. We saw in §5 that doing so does not scale to the WAN topologies of today or the future, which consist of thousands of sites; (2) We saw that approximate algorithms for multi-commodity max flow, such as [27], require a large number of switch forwarding entries since they can send flow along any edge. Also, NCFlow allocates more flow and is faster compared to path-based versions of these algorithms. (3) Probabilistic fault protection schemes such as TEAVAR [19] take infeasibly long to run on large topologies when considering multiple link failures; they also allocate less flow to reserve capacity to deal with possible failures. Other oblivious techniques [13,14,19,44,49,66] have a similar tradeoff. Quickly recomputing using NCFlow trades off slightly more loss after a fault to carry much more traffic before the fault and after recomputation; hence, we believe that NCFlow is better suited to enterprise WANs, which target very high link utilization and have traffic that is elastic to short-term loss (e.g., scavenger-class traffic, such as replicating large datasets [35, 38, 49]). Here, we discuss other related work.

TE on WANs: Typically, a WAN node is not a single switch, but rather a group of switches connected in a specific way such as a full mesh. Similarly, a WAN edge is a systematic collection of links between many switches. [36] discusses how to hide the intra-node connectivity from the global TE solution. NCFlow complements this technique; it can use a similar intra-node scheme and can support WANs that are 10× larger than were considered in [36]. The specific contraction used by NCFlow—node clusters with large capacity and/or demand between themselves—also differs from the contractions used in route planning [4, 9, 15]. Some BGP-based TE schemes [24, 62, 69], which address how best to move traffic between different (BGP) domains, are also complementary to NCFlow which considers the WAN of a single enterprise (domain). Other TE schemes use different protocols, such as OSPF, or work over longer timescales (e.g., hours to days) [29, 39, 46, 51].

Multi-Commodity Flow Solutions: Both the edge- and path-based LP formulations are well-studied [16, 67]. Some works consider the case of a single commodity, i.e., one source and target, and do not directly extend to the case of multiple commodities [34,48,55]. The best-known approximate algorithms for multi-commodity flow problems incrementally allocate flow on the shortest path and increase the length of all edges on that path [17, 27, 30, 41]. For the problem sizes considered here, LP solvers such as Gurobi are faster in practice, perhaps because they take larger steps towards the optimal allocation. A few works customize LP solvers to improve performance on flow problems [23, 50]. NCFlow is agnostic to the solver used and can use any solver for the sub-problems in Figure 6.

Decompositions: Using standard decomposition techniques for large optimization problems, such as Dantzig-Wolfe and Benders [16,20], for multi-commodity flow problems has lead to inconclusive results [31,54]; i.e., not consistently faster than MaxFlow. NCFlow can be thought of as a problem-specific decomposition that leverages the observation that both capacity and demands are concentrated in today's WANs.

8 Conclusion

We present a fast and practical solution for allocating flow on large WANs. We leverage the concentrated nature of demands and topologies to divide nodes into clusters and solve sub-problems per cluster and on the aggregated graph. Our heuristics guarantee feasibility and empirically achieve close-to-optimal flow allocations. By reusing pathlets and splitting rules across demands, we require fewer forwarding entries in switches. Empirically, on topologies that are over 10× larger than were considered in prior work and many traffic matrices, our solution NCFlow is 8.2× faster than the state of the art, while allocating 98.8% of the total flow and using 6× fewer forwarding entries in the median case. We demonstrate that NCFlow offers sizable benefits when tracking changing demands and reacting to failures. As enterprise WANs continue to grow, we believe techniques such as NCFlow can enable improved traffic orchestration and higher link utilization.

References

[1] Capacity planning for the Google backbone network. https://bit.ly/2lViJ4t.

[2] Code for NCFlow and Baselines. https://github.com/netcontract/ncflow.

[3] Code for TEAVAR. https://github.com/manyaghobadi/teavar.

[4] Contraction Hierarchies Path Finding Algorithm. https://bit.ly/3eaiqtg.

[5] GAP: Generalizable Approximate Graph Partitioning Framework. https://arxiv.org/pdf/1903.00614.pdf.

[6] Internet Topology Zoo. http://www.topology-zoo.org/.

[7] Market Trends: SD-WAN and NFV for Enterprise Network Services. https://gtnr.it/3c8hNyA.

[8] Cristinel Ababei. Code for Karakostas. https://bit.ly/2woSloP.

[9] Ittai Abraham, Daniel Delling, Andrew V. Goldberg, and Renato F. Werneck. A Hub-Based Labeling Algorithm for Shortest Paths in Road Networks. In *Experimental Algorithms*, 2011.

[10] Firas Abuzaid, Srikanth Kandula, Behnaz Arzani, Ishai Menache, Matei Zaharia, and Peter Bailis. Solving Flow Problems Quickly by Contracting Wide-area Network Topologies: Extended Version. https://bit.ly/35oyQdU.

[11] Ravindra Ahuja, Thomas Magnanti, and James Orlin. *Network Flows. Theory, Algorithms, and Applications*. Prentice Hall.

[12] Muthukaruppan Annamalai et al. Sharding the Shards: Managing Datastore Locality at Scale with Akkio. In *OSDI*, 2018.

[13] D. Applegate, L. Breslau, and E. Cohen. Coping with Network Failures: Routing Strategies for Optimal Demand Oblivious Restoration. In *SIGMETRICS*, 2004.

[14] David Applegate and Edith Cohen. Making Intra-Domain Routing Robust to Changing and Uncertain Traffic Demands. In *SIGCOMM*, 2003.

[15] Hannah Bast, Daniel Delling, Andrew V. Goldberg, Matthias Müller-Hannemann, Thomas Pajor, Peter Sanders, Dorothea Wagner, and Renato F. Werneck. Route Planning in Transportation Networks. *CoRR*, 2015.

[16] Dimitris Bertsimas and John N Tsitsiklis. *Introduction to linear optimization*, volume 6. Athena Scientific Belmont, MA, 1997.

[17] Daniel Bienstock. *Potential function methods for approximately solving linear programming problems: theory and practice*, volume 53. Springer Science & Business Media, 2002.

[18] Vincent D Blondel, Jean-Loup Guillaume, Renaud Lambiotte, and Etienne Lefebvre. Fast unfolding of communities in large networks, 2008.

[19] Jeremy Bogle et al. TEAVAR: striking the right utilization-availability balance in WAN traffic engineering. In *SIGCOMM*, 2019.

[20] Stephen Boyd and Lieven Vandenberghe. *Convex Optimization*. Cambridge University Press, 2004.

[21] P. Brucker. On the complexity of clustering problems. In *Optimizing and Operations Research*, Berlin, West Germany, 1977. Springer-Verlag.

[22] Yiyang Chang, Sanjay Rao, and Mohit Tawarmalani. Robust validation of network designs under uncertain demands and failures. In *NSDI*, 2017.

[23] P. Chardaire and A. Lisser. Simplex and Interior Point Specialized Algorithms for Solving Nonoriented Multicommodity Flow Problems. *Operations Research*, 2002.

[24] David Chou, Tianyin Xu, Kaushik Veeraraghavan, Andrew Newell, Sonia Margulis, Lin Xiao, Pol Mauri Ruiz, Justin Meza, Kiryong Ha, Shruti Padmanabha, et al. Taiji: Managing Global User Traffic for Large-Scale Internet Services at the Edge. In *OSDI*, 2019.

[25] A. Clauset, M.E.J. Newman, and C. Moore. Finding community structure in very large networks. *Phys. Rev.*, 2004.

[26] Aaron Clauset. Fast Modularity Community Structure Inference Algorithm. https://bit.ly/3aAVGQH.

[27] Lisa K. Fleischer. Approximating Fractional Multicommodity Flow Independent of the Number of Commodities. *SIAM J. Discret. Math.*, 2000.

[28] Ken Florance. How Netflix Works With ISPs Around the Globe to Deliver a Great Viewing Experience. https://bit.ly/2RYYrEM, 2016.

[29] B. Fortz and Mikkel Thorup. Internet Traffic Engineering by Optimizing OSPF Weights in a Changing World. In *INFOCOM*, 2000.

[30] Naveen Garg and Jochen Könemann. Faster and Simpler Algorithms for Multicommodity Flow and Fractional Packing Problems. *SIAM J. Comput.*, 2007.

[31] A. M. Geoffrion and G. W. Graves. Multicommodity Distribution System Design by Benders Decomposition. *Management Science*, 1974.

[32] P. Brighten Godfrey, Igor Ganichev, Scott Shenker, and Ion Stoica. Pathlet routing. In *SIGCOMM*, 2009.

[33] Zonghao Gu, Edward Rothberg, and Robert Bixby. Gurobi optimizer reference manual, version 5.0. *Gurobi Optimization Inc., Houston, USA*, 2012.

[34] Jeff Hartline and Alexa Sharp. Hierarchical Flow. Technical Report 2004-09-29, Cornell University, 2004.

[35] Chi-Yao Hong, Srikanth Kandula, Ratul Mahajan, Ming Zhang, Vijay Gill, Mohan Nanduri, and Roger Wattenhofer. Achieving high utilization with software-driven WAN. In *SIGCOMM*, 2013.

[36] Chi-Yao Hong, Subhasree Mandal, Mohammad Al-Fares, Min Zhu, Richard Alimi, Chandan Bhagat, Sourabh Jain, Jay Kaimal, Shiyu Liang, Kirill Mendelev, et al. B4 and after: managing hierarchy, partitioning, and asymmetry for availability and scale in google's software-defined WAN. In *SIGCOMM*, 2018.

[37] Yuanfang Hu, Yi Zhu, Hongyu Chen, Ronald L. Graham, and Chung-Kuan Cheng. Communication latency aware low power NoC synthesis. In *DAC*, 2006.

[38] Sushant Jain, Alok Kumar, Subhasree Mandal, Joon Ong, Leon Poutievski, Arjun Singh, Subbaiah Venkata, Jim Wanderer, Junlan Zhou, and Min Zhu. B4: Experience with a globally-deployed software defined WAN. In *SIGCOMM*, 2013.

[39] Virajith Jalaparti, Ivan Bliznets, Srikanth Kandula, Brendan Lucier, and Ishai Menache. Dynamic pricing and traffic engineering for timely inter-datacenter transfers. In *SIGCOMM*, 2016.

[40] S. Kandula, I. Menache, R. Schwartz, and S. R. Babbula. Calendaring for Wide Area Networks. In *SIGCOMM*, 2014.

[41] George Karakostas. Faster Approximation Schemes for Fractional Multicommodity Flow Problems. *ACM Trans. Algorithms*, 2008.

[42] Robert Krauthgamer, Joseph (Seffi) Naor, and Roy Schwartz. Partitioning Graphs into Balanced Components. In *SODA*, 2009.

[43] Alok Kumar et al. Bwe: Flexible, hierarchical bandwidth allocation for wan distributed computing. In *SIGCOMM*, 2015.

[44] Praveen Kumar et al. Semi-Oblivious Traffic Engineering: The Road Not Taken. In *NSDI*, 2018.

[45] Praveen Kumar, Chris Yu, Yang Yuan, Nate Foster, Robert Kleinberg, and Robert Soulé. YATES: Rapid Prototyping for Traffic Engineering Systems. In *SOSR*, 2018.

[46] Nikolaos Laoutaris, Michael Sirivianos, Xiaoyuan Yang, and Pablo Rodriguez. Inter-datacenter Bulk Transfers with NetStitcher. In *SIGCOMM*, 2011.

[47] David Lebrun, Mathieu Jadin, François Clad, Clarence Filsfils, and Olivier Bonaventure. Software Resolved Networks: Rethinking Enterprise Networks with IPv6 Segment Routing. In *SOSR*, 2018.

[48] Chansook Lim, S. Bohacek, Joao Hespanha, and Katia Obraczka. Hierarchical Max-Flow Routing. In *Globecom*, 2005.

[49] Hongqiang Harry Liu, Srikanth Kandula, Ratul Mahajan, Ming Zhang, and David Gelernter. Traffic engineering with forward fault correction. In *SIGCOMM*, 2014.

[50] Richard McBride. Progress Made in Solving the Multicommodity Flow Problem. *SIAM Journal on Optimization*, 1998.

[51] Srinivas Narayana, Joe Jiang, Jennifer Rexford, and Mung Chiang. Distributed Wide-Area Traffic Management for Cloud Services. In *SIGMETRICS*, 2012.

[52] NetworkX. Edge Disjoint Paths. https://bit.ly/37VJ71k.

[53] Andrew Y Ng, Michael I Jordan, and Yair Weiss. On spectral clustering: Analysis and an algorithm. In *NIPS*, 2002.

[54] Murat Oguz, Tolga Bektas, and Julia A. Bennell. Multicommodity flows and Benders decomposition for restricted continuous location problems. *European Journal of Operational Research*, 2017.

[55] James Orlin. A polynomial time primal network simplex algorithm for minimum cost flows. *Math. Programming*, 1997.

[56] Qifan Pu, Ganesh Ananthanarayanan, Peter Bodik, Srikanth Kandula, Aditya Akella, Victor Bahl, and Ion Stoica. Low Latency Geo-distributed Data Analytics. In *SIGCOMM*, 2015.

[57] H Racke. Optimal Hierarchical Decompositions for Congestion Minimization in Networks. In *STOC*, 2008.

[58] R Tyrrell Rockafellar and Stanislav Uryasev. Conditional Value-at-Risk for General Loss Distributions. *Journal of banking & finance*, 26(7):1443–1471, 2002.

[59] E. Rosen, A. Viswanathan, and R. Callon. Multi-Protocol Label Switching Architecture. RFC 3031.

[60] Matthew Roughan, Albert Greenberg, Charles Kalmanek, Michael Rumsewicz, Jennifer Yates, and Yin Zhang. Experience in Measuring Backbone Traffic Variability: Models, Metrics, Measurements and Meaning. In *IMW*, 2002.

[61] S. Kandula and D. Katabi and S. Sinha and A. Berger. Dynamic Load Balancing Without Packet Reordering. In *CCR*, 2006.

[62] Brandon Schlinker et al. Engineering Egress with Edge Fabric: Steering Oceans of Content to the World. In *SIGCOMM*, 2017.

[63] Submarine Cable Map. http://www.submarinecablemap.com.

[64] Asaf Valadarsky, Michael Schapira, Dafna Shahaf, and Aviv Tamar. Learning to Route. In *Proceedings of the 16th ACM Workshop on Hot Topics in Networks*, HotNets, 2017.

[65] Santosh Vempala, Ravi Kannan, and Adrian Vetta. On Clusterings Good, Bad and Spectral. In *FOCS*, 2000.

[66] Hao Wang, Haiyong Xie, Lili Qiu, Yang Richard Yang, Yin Zhang, and Albert Greenberg. COPE: Traffic Engineering in Dynamic Networks. In *SIGCOMM*, 2006.

[67] I-Lin Wang. Multicommodity Network Flows: A Survey, Part I: Applications and Formulations. *Internal Journal of Operations Research*, 2018.

[68] Mathieu Xhonneux, Fabien Duchêne, and Olivier Bonaventure. Leveraging eBPF for programmable network functions with IPv6 Segment Routing. In *CoNext*, 2018.

[69] Kok-Kiong Yap et al. Taking the edge off with espresso: Scale, reliability and programmability for global internet peering. In *SIGCOMM*, 2017.

[70] Jin Yen and NetworkX. K-Shortest Paths. https://bit.ly/2OpNGJn.

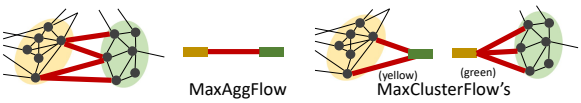

Figure 17: Considering the crossing edges between the yellow and green clusters from Figure 2; MaxAggFlow has a single bundle; the yellow and green instances of MaxClusterFlow have one bundle for each incident node in their cluster.

A More Discussion

NCFlow is **agnostic to the underlying solver** used for the problems in Figure 6 and can benefit from future improvements to LP solvers and approximate methods [27, 30, 41].

Further use cases: Beyond serving as a drop-in replacement for today's production WAN traffic controllers, NCFlow can be used whenever fast and close-to-optimal solutions are desirable such as: when allocating flow for future time-steps [39, 40] or to compare topology changes [1, 22] or to accelerate the training of ML-based routing systems [64].

B Properties of NCFlow's flow allocation algorithm

B.1 Proof that the algorithm in §3.1 meets demand and capacity constraints

Satisfying demand constraints: Demands whose source and target are in the same cluster are considered by only one instance of MaxClusterFlow; hence, they do not receive more flow than their demands. Specifically, MaxClusterFlow in Figure 6 invokes MaxFlow which in turn imposes the demand constraints listed in FeasibleFlow; Equation 1.

Demands whose source and target are in different clusters receive no more flow than their demand due to SrcTargetMax; observe in Figure 6 that one of the four constraints in SrcTargetMax explicitly controls the flow for such demands.

Satisfying edge capacity constraints: We say an edge is local to a cluster if both its incident nodes are within the same cluster. Flow is assigned to a local edge only by the MaxClusterFlow instance of the cluster that contains that edge. Since MaxClusterFlow ultimately invokes FeasibleFlow; by Equation 1 a local edge is allocated no more than its capacity.

Edges that are not local receive flow allocation in MaxAggFlow where, as noted in §3.1, all of the edges that lie between a pair of clusters are treated as a single edge whose capacity equals the sum of the capacity of the underlying edges. Thus, the flow assigned to a bundle of edges by MaxAggFlow is no more than the total capacity of the edges in the bundle. Subsequently, MaxClusterFlow instances behave similarly; that is, the flow allocated for a bundle of edges is no more than the capacity of that bundle. For example, Figure 17 shows the four edges between the yellow and green clusters in Figure 2 as well as the bundles considered by MaxAggFlow (in the

middle) and the two instances of MaxClusterFlow corresponding to the yellow and green clusters on the right. The later steps in Figure 6 do not increase flow and so we conclude that capacity constraints are satisfiable for all non-local edges.

B.2 Proof that the heuristic in §3.2 leads to feasible flow allocations

Here, we prove Theorem 1. First, note that the heuristic in §3.2 which only restricts the edges between clusters and paths on the aggregate graph that can be used by some demands does not affect the proof in §B.1; that is, edges still receive flow less than their capacity and demand constraints hold.

We now prove that the heuristic will satisfy flow conservation; that is, at any node in the network, for any demand which neither originates nor ends at this node, the net flow is zero, i.e., incoming flow to the node equals the flow leaving that node.

It is easy to see that flow conservation holds for demands whose source and target are in the same cluster even without the heuristic in §3.2 because: (1) Only the instance of MaxClusterFlow for that cluster assigns flow to such a demand. (2) Since MaxClusterFlow invokes FeasibleFlow in Equation 1, the flow is allocated along paths which start and end at the source and target of that demand respectively. (3) Thus, every node that is neither the source or target will have incoming flow equal to the outgoing flow.

We now consider the remaining demands, that is, whose source and target are in different clusters.

It is easy to see that for such demands, flow conservation holds at all nodes that do not have edges to or from other clusters by logic that is similar to the above. The MaxClusterFlow instance of the cluster containing such a node would allocate flow to some bundle of demands on paths in this cluster that neither start nor end at such a node.

The only case left is nodes which have edges to and from other clusters. Suppose by contradiction that some demand k violates flow conservation at such a node u. The heuristic in §3.2 allocates flow for demand k along only one path in the aggregated graph and on only one edge between connected clusters. If the cluster containing u is not on the chosen path or none of the chosen edges are incident on u, then the net flow allocated for k over all edges incident on u will be zero. Let e be that one chosen crossing edge incident on u which can receive non-zero flow for demand k. Observe that all of the other demands whose source and target are in the same clusters as k would also be allocated flow on the same path and edges as k. Thus, all the flow allocated for these demands entering or leaving node u as the case may be would be on edge e. Two instances of MaxClusterFlow, one corresponding to the cluster that contains u and another corresponding to the other side of edge e, will assign possibly different flow values for this bundle of demands on edge e. To conclude our proof, note that MinPathE2E takes the minimum flow assigned along all such crossing edges e on the chosen path through the aggregated graph and that SrcTargetMax further breaks open the bundle to assign feasible flow for each actual demand contained in the bundle.

If more than one crossing edge or more than one path on the aggregate graph are used for a demand, it is easy to see how the above proof will break. The two instances of MaxClusterFlow that correspond to the clusters on either side of a crossing edge will be forced by MinPathE2E to only agree on the total volume for the cluster bundle of demands for all edges between the pair of clusters; that is, these instances may allocate different flow on different edges or allocate different flow to individual demands in the bundle. Figure 8 shows simple examples of such disagreement.

B.3 Proof of optimality for algorithm in §3.1 given some sufficient conditions

Here, we prove Theorem 2. We already discussed in §3.3 the case where the number of clusters, η, is 1 or N, the number of nodes in the graph. To prove optimality for the other sufficient conditions, we posit a helper theorem.

Theorem 3. *Given a set of paths $\mathcal{P}$ that can be used by flows, there exists a clustering of nodes into clusters such that any flow allocated on a set of paths $\mathcal{P}$ can also be allocated by the method in Figure 6 over those clusters.*

Proof. The claim is trivially true by using N clusters, where each node is in a cluster by itself. We show that it is possible to use fewer clusters next. Let $\mathcal{S}$ be a set of nodes such that every path in $\mathcal{P}$ contains at most one contiguous sequence of the nodes in $\mathcal{S}$. For example, the set $\{u, v\}$ satisfies this property if every path in $\mathcal{P}$ has neither u nor v, just u but not v (no repetitions allowed), just v but not u, $u \to v$ (no repetitions of u or v anywhere else in the path) or $v \to u$. Coalescing each such set $\mathcal{S}$ into a cluster would allow the method in Figure 6 to allocate the same flow as MaxFlow using the paths in $\mathcal{P}$. □

If G_{agg} is a tree and there is at most one edge between any pair of clusters, any set of paths $\mathcal{P}$ on the actual graph would consist of contiguous segments that are contained within each cluster. Thus, per the above theorem, any flow allocated by MaxEdgeFlow (Equation 6) can also be allocated by the method in Figure 6. The only difference then between the global optimization and the method in Figure 6 is that whereas the former is a single optimization call, the latter is a sequence of optimizations. Since demands are satisfiable, however, all of the steps in Figure 6 will allocate the entirety of demand and hence will allocate the maximum amount of flow.

Note, in particular, that for the sufficient conditions listed in Theorem 2 a single iteration of the steps in Figure 6 suffice.

In §H, we show some counter-examples where NCFlow can lead to sub-optimal allocations when any of these sufficient conditions do not hold.

C Data-plane details for NCFlow

C.1 Actions at the NCFlow controller, after each allocation

The SDN controller for NCFlow computes total flow per demand and some splitting ratios after each allocation.

Total Flow: The flow assigned to a demand whose source and target are in different clusters is read off SrcTargetMax, i.e., $f_{4,k}$. For intra-cluster demands, their flow is read off MaxClusterFlow, i.e., $f^x_{2,k}$ at the cluster x that contains the source and target of demand k. These flow values are summed up over all the iterations used by NCFlow.

Splitting ratios at sources: At source s of cluster x, we have two cases depending on whether the target of the demand is within the cluster x or in some other cluster y.

For the former case, let $\mathcal{P}_{st}$ be the path set to target t for demand k; the splitting ratio for each path p in the set is $f^{x,p}_{2,k}$ summed up over all iterations, divided by the total flow assigned to demand k above. Here, $f^{x,p}_{2,k}$ is the flow assigned to demand k on path p by the MaxClusterFlow instance for cluster x.

For the latter case, let z_i be the next cluster on the one path that can receive flow in iteration i for all traffic going to targets in cluster y. The splitting ratio for path p in the path set $\bigcup_i \mathcal{P}_{sz_i}$ is the value of $\sum_{r\in K_{sy}} f^{x,p}_{2,r}$ summed up over all iterations where K_{sy} is the set of all demands from source s to targets in cluster y divided by the total value for all such paths.

Uniquely, note that each source s has a splitting ratio per target t within the same cluster or per target cluster y.

We call a subset of nodes as ingresses if they have at least one edge to a node in another cluster that is chosen by the offline component of NCFlow in §3.4 as a crossing edge

Splitting ratios at ingresses are computed in a similar way to the splitting ratios at sources. At each ingress node w of cluster y for traffic from cluster x, there are two cases depending on whether the target is some node t in the same cluster as the ingress (y) or in some other cluster z.

For the former case, in iteration i, the splitting ratio for path p in the set $\mathcal{P}_{wt}$ is the value of $\sum_{r\in K_{xt}} f^{y,p}_{2,r}$ in iteration i divided by the total over all such paths. As above, K_{xt} is the set of demands from sources in cluster x to target t.

For the latter case, in iteration i, let z_i be the next cluster on the path to targets in z; the splitting ratio for path p in the set $\mathcal{P}_{wz_i}$ is the value of $\sum_{r\in K_{xz}} f^{y,p}_{2,r}$ divided by the total value over all such paths. As above, K_{xz} is the set of all demands from sources in cluster x to targets in cluster z.

Note that an ingress node w has splitting ratios only for demands whose chosen path at an iteration contains w's cluster (y) and whose chosen edge enters y at w.

C.2 Details on switch forwarding entries

Pathlets: NCFlow sets up label-switched paths (LSPs) between each pair of nodes in each cluster. Which paths to setup is pre-determined by the offline component in §3.4.

Splitting rules: A source s in cluster x has a splitting rule for each other node in the same cluster and for each other cluster. The splitting ratios are as computed in §C.1.

In each iteration, at each cluster, at most one ingress node is active per pair of other clusters. This is because the bundle of demands for a given pair of clusters has at most one crossing edge entering a cluster.

The active ingress node at a cluster x for the bundle of demands from cluster y to cluster z has one splitting rule when $z \neq x$ and one splitting rule per target in cluster x when $z = x$.

Packet content: The LSP (which pathlet to use) is encoded in the L2 header [59]. Additionally, NCFlow has the following tuple in each packet: (x, y, i, e) where x and y are the source and target cluster ids, i is the iteration number of the flow allocation that the packets have been assigned to and e is the edge to leave the current cluster on. The bits needed are $2\ln\eta + \ln I + \ln$ node degree.[5] We note that 16 bits of header space suffice for all the WAN topologies and experiments considered in this paper; that is $\eta \leq 64$ clusters, $I \leq 8$ iterations and up to 2 edges to nodes in other clusters being used per egress node by NCFlow.

Data path actions:

- At source s in cluster x:
  - The host or middleware adds the cluster-ids x and y into the packet.
  - Source switch uses the appropriate splitting rule to pick a (p, i, e) tuple; the values e and i are placed in the packet and the L2 header gets the identifier for path p. To avoid reordering packets in the same TCP flow, traffic can be split using flow hashes or flowlets [61].
- Each cluster egress removes e from the packet header and forwards packets to the next-hop of the edge e.
- Each cluster ingress uses the appropriate splitting rule to pick a (p, e) tuple; the value e is put into the packet header and p determines the identifier in the L2 header.

D Definitions of NoMoreFlow

In the flow vector computed by MaxClusterFlow at a cluster x, $\mathbf{f^x_2}$, we use the subscript k to denote a bundle that may include (1) transit demands through cluster x (i.e., from all sources in some other cluster w to targets in some other cluster z), (2) leaving demands (i.e., from a source in cluster x to

[5] The edge id must suffice to distinguish at an egress node between the edges to a particular next cluster; so node degree is an overestimate.

all targets in some other cluster z) or (3) entering demands (i.e., to a target in cluster x from all sources in some other cluster z). Furthermore, we use the subscript y_{out} to denote the flow allocated for the bundle k on paths to the virtual node that corresponds to the cluster y. Thus, $f^x_{2,k,y_{\text{out}}}$ is the flow allocated at cluster x for all demands in the per-cluster bundle k on paths to the virtual node corresponding to a neighboring cluster y.

With this background, Equation 3 ensures that the flows allocated in MinPathE2E for an inter-cluster bundle K in $\mathcal{D}_{\text{agg}}$ on all paths in $\mathcal{P}_{\text{agg}}$ that contain a cluster edge (x,y) is no more than the flow that is allocated at either cluster x or cluster y for their respective per-cluster bundles that are contained in K to and from each other respectively.

$$\text{NoMoreAlongPaths}(\mathbf{f},\mathbf{f_2}) \triangleq \forall K \in \mathcal{D}_{\text{agg}},\ \forall x,y \in \mathcal{V}_{\text{agg}}, x \neq y,$$
$$\sum_{p \in \mathcal{P}_{\text{agg}},(x,y)\in p} f^p_K \leq \min\left(\sum_{k\in K} f^x_{2,k,y_{\text{out}}}, \sum_{k'\in K} f^y_{2,k',x_{\text{in}}}\right) \tag{3}$$

Equation 4 is logically similar to Equation 3 except that the constraints are specific to a cluster x and the constants and variables have been flipped; that is, here, the flows on the paths in the aggregate graph are given ($f^p_{1,K}$) and the flow on paths within the cluster are to be computed by MaxClusterFlow. In particular, note that $\sum_{p'\in\mathcal{P}_{x,*y}} f^{p'}_k \triangleq f^x_{2,k,y_{\text{out}}}$; that is, the flow assigned in MaxClusterFlow of cluster x on all paths leading to the virtual node corresponding to a neighbor cluster y is precisely the value on the right that is used above in Equation 3.

$$\text{NoMoreFlowThruCluster}(\mathbf{f},\mathbf{f_1},x) \triangleq \forall K \in \mathcal{D}_{\text{agg}},\ \forall y \in \mathcal{V}_{\text{agg}} : y \neq x,$$
$$\sum_{p\in\mathcal{P}_{\text{agg}}:(y,x)\in p} f^p_{1,K} \geq \sum_{k\in K,\ p'\in\mathcal{P}_{x,y_{\text{in}^*}}} f^{p'}_k, \text{ and}$$
$$\sum_{p\in\mathcal{P}_{\text{agg}}:(x,y)\in p} f^p_{1,K} \geq \sum_{k\in K,\ p'\in\mathcal{P}_{x,*y_{\text{out}}}} f^{p'}_k \tag{4}$$

E Fault Model

When failures happen, prior works [19, 49] assume that the sources of the label switched paths (LSPs) will proportionally shift traffic. That is, a source that splits traffic in the ratio of $(0.3, 0.5, 0.2)$ between three paths will change to a splitting ratio of $(0.6, 0, 0.4)$ when the middle LSP fails. Doing so can cause congestion on either of the remaining LSPs.

The key idea in prior works [19, 49] is to proactively allocate flow such that the maximal load on any link remains under capacity—FFC [49] protects against up to k simultaneous link failures, whereas TEAVAR [19] ensures that the flow at risk is below a given fraction (e.g., 99.9% of flow can be carried by the network on average over all possible failure scenarios).

The cost of such congestion protection is two-fold: (1) proactive schemes substantially increase the solution runtime, and (2) they under-allocate flow, since capacity must be set aside to help with possible failures. Instead, NCFlow uses a *reactive* strategy, and recomputes a new flow allocation after the fault occurs. This enables NCFlow to carry more flow before the fault, and potentially carry more flow after recovery. Furthermore, since NCFlow uses fewer FIB entries for the same number of paths, it is naturally easier to spread flow onto more paths with NCFlow. Thus, the key trade-off is slightly longer and more lossy episodes immediately after a fault when using NCFlow versus longer solver runtimes and flow under-allocation with proactive schemes [19, 49].

F Benchmarking TEAVAR and TEAVAR*

F.1 Formulation for TEAVAR*

Here, we discuss our adaptation of TEAVAR to maximize total multi-commodity flow. The TEAVAR [19] paper considers a different objective – maximizing the *concurrent* multi-commodity flow (see Table 2). When all demands are satisfiable, both objectives allocate the same flow; however, when not enough capacity is available to meet the desired failure assurance, maximizing total flow leads to a strictly larger allocation. We describe TEAVAR* from first principles here.

In addition to the inputs of MaxFlow (see Equation 2), TEAVAR* has the following inputs:

- A value $\beta \in [0,1]$; larger values of β correspond to greater fault assurance.
- A set of fault scenarios, $\mathcal{S}$; each scenario i has a probability of occurrence β_i and a set of failed edges $\mathcal{E}_i$.

In a fault scenario i, the edges in $\mathcal{E}_i$ will fail and so the flow allocated to paths that contain any edge in $\mathcal{E}_i$ will be *lost*. The number of possible fault scenarios is exponential in the number of edges in the network. Thus, to keep the optimization tractable, we consider only a subset of scenarios.

Let $\mathcal{L}(i)$ denote the total flow lost in fault scenario i. Per Proposition 8 in [58], minimizing the potential function, $\alpha + \frac{1}{1-\beta}\mathbb{E}[\mathcal{L}_i - \alpha]^+$, would minimize the conditional value at risk. Here, the expectation is over all possible fault scenarios. Since we only consider a subset of fault scenarios to keep optimization tractable, we minimize: $\alpha + \frac{1}{1-\beta}\left(\sum_{i\in\mathcal{S}}\beta_i[\mathcal{L}_i-\alpha]^+ + (1-\sum_{i\in\mathcal{S}}\beta_i)(1-\alpha)\right)$. The last term accounts for the unconsidered scenarios for which we must assume the worst possible loss. Note that we can simplify this expression by dropping the constant $\frac{1-\sum_{i\in\mathcal{S}}\beta_i}{1-\beta}$.

$$\begin{aligned}
&\text{TEAVAR}^*(\mathcal{V},\mathcal{E},\mathcal{D},\mathcal{P},\beta,\mathcal{S}) && && (5)\\
&\triangleq \arg\min_{\mathbf{f}} \left(\alpha + \tfrac{1}{1-\beta}\left(\textstyle\sum_{i\in\mathcal{S}} \beta_i \text{Excess}_i - (1-\textstyle\sum_{i\in\mathcal{S}}\beta_i)\alpha\right)\right)\\
&\text{s.t. } \mathbf{f} \in \quad \text{FeasibleFlow}(\mathcal{V},\mathcal{E},\mathcal{D},\mathcal{P}), && && \text{(Eqn. 1)}\\
&\quad \mathcal{L}_{i,k} \geq 0, && \forall i,k && \text{(loss is non-negative)}\\
&\quad \mathcal{L}_{i,k} \geq d_k - \sum_{p\in\mathcal{P}_k} f_k^p \text{Active}_{p,i}, && \forall i,k && \text{(loss)}\\
&\quad \alpha \geq 0 && && \text{(loss } \textit{cutoff}\text{)}\\
&\quad \text{Excess}_i \geq 0 && \forall i && \text{(excess loss in scenario } i\text{)}\\
&\quad \text{Excess}_i \geq \sum_{k\in\mathcal{D}} \mathcal{L}_{i,k} - \alpha, && \forall i && \text{(excess loss)}
\end{aligned}$$

The formulation for TEAVAR* is in Equation 5. Recall that f_k^p is the flow assigned to demand k on path p. $\text{Active}_{p,i}$ is an indicator denoting whether path p is active in fault scenario i. Thus, the allocation for demand k in scenario i will be $\sum_{p\in\mathcal{P}_k} f_k^p \text{Active}_{p,i}$. When the allocation is below the required volume d_k, the demand will suffer loss; we use $\mathcal{L}_{i,k}$ to denote the flow loss for demand k in scenario i.

The flow allocation resulting from the above formulation cannot be promised to the demands; in particular, more flow will be assigned on some paths to account for possible failures on other paths. After solving the above LP, we compute the flow allocation for a demand k as follows: (1) sort the per-scenario losses $\mathcal{L}_{i,k}$ in ascending order; (2) starting at index 0, add up the probability of each scenario until the running sum is at least β—let i_β be the unique crossing index; (3) Set demand k's flow to be $d_k - \mathcal{L}_{i_\beta,k}$, the demand minus the loss at the crossing index.

Choosing the fault scenarios to use in TEAVAR*:

- Intuitively, achieving a greater amount of fault assurance requires considering more fault scenarios. Specifically, if the total probability of considered scenarios is below β, the above LP as well as the LP used by TEAVAR become unbounded. To see why, the coefficient of α in Eqn. 5 is $\frac{(\sum_{i\in\mathcal{S}}\beta_i)-\beta}{1-\beta}$. If the probability of considered scenarios is less than β, this coefficient becomes negative, and the objective value reaches $-\infty$ by setting α to ∞.
- Intuitively, if the total probability of considered scenarios is just larger than β, the flow allocated to demands is very small. To see why, the smaller the value of $\sum_{i\in\mathcal{S}}\beta_i - \beta$, the smaller the positive coefficient of α in the objective of Eqn 5. Thus, the solution of Eqn 5 will have a large value of α and a very small amount of allocatable flow.
- In light of these two points, in our experiments, we choose all scenarios that are individually more likely to occur than a cutoff ρ and multiplicatively reduce ρ until the total probability of considered scenarios exceeds $1-\frac{1-\beta}{2}$.

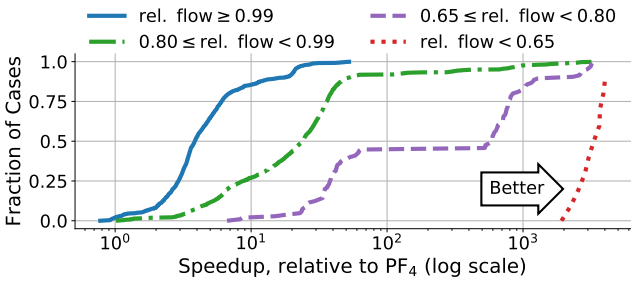

Figure 18: Breaking down the NCFlow results from Figure 11b into four separate CDFs based on relative total flow.

F.2 Comments on benchmarking TEAVAR

Observe that the number of scenarios affects the complexity of the TEAVAR* optimization; specifically, the number of equations and variables increases by $|\mathcal{S}| * |\mathcal{P}|$. The path set is at least as large as the node pairs, i.e., $|\mathcal{P}| > N^2$ where N is the number of nodes. The appropriate choice of fault scenarios to consider, as discussed above, depends on the size of the topology, the failure probability of edges, and the required assurance level β. Suppose one considers all 2-edge failure scenarios; then $|\mathcal{S}| \sim M^2$ where M is the number of edges. Hence, the increase in equations and variables exceeds N^2M^2. Note that MaxFlow is substantially simpler, having at most $O(N^2)$ variables and constraints (Equation 1).

On the topologies listed in Table 5, our implementation of TEAVAR* never ran to completion even after several days. We ran with $\beta = 0.99$ and link failure probability set to 0.004; both of these are the default values used in [3]. The reason is that the optimization problem becomes intractably large. TEAVAR behaves similarly [19]. We conclude that probabilistic fault protection using this methodology is infeasible on large topologies and for non-trivial fault assurance levels such as when considering multiple link failures.

We also note that we are unable to simultaneously achieve the solution quality and the runtimes that are reported in TEAVAR [19] using their code [3]. Specifically, achieving the assurance levels reported in their experiments requires many scenarios to be considered. The runtimes reported in [19] appear to have been measured when considering only single link failures.

G Additional Experiments

G.1 Breakdown of NCFlow's Performance

To further understand the performance of NCFlow, Figure 18 breaks down the results in Figure 11 into four ranges based on total relative flow. We plot CDFs of the speedup ratio per range. The solid blue and green dashed line, which correspond to relative flow above 0.99 and in $[0.8, 0.99)$ respectively, account for 49% and 46% of all experiments. The figure shows that NCFlow achieves sizable speedups while allocating large

Topology	Edge-Based	Räcke	KSP	NCFlow
Total # FIB Entries				
PrivateLarge	945,038,502	52,515,090	22,483,244	**1,694,027**
Kdl	427,524,786	76,794,001	30,199,751	**1,876,289**
PrivateSmall	7,684,182	1,232,866	625,282	**139,346**
Cogentco	7,567,952	2,054,323	915,207	**139,862**
UsCarrier	3,894,542	1,520,821	510,894	**82,301**
Colt	3,534,912	1,048,779	346,905	**67,307**
GtsCe	3,263,696	1,077,350	535,135	**101,368**
TataNld	3,006,720	1,062,629	540,088	**93,179**
DialtelecomCz	2,590,122	1,427,780	529,663	**83,128**
Ion	1,922,000	886,414	418,362	**71,614**
Deltacom	1,417,472	459,159	246,811	**53,948**
Interoute	1,306,910	483,960	249,979	**32,193**
Uninett2010	394,346	133,742	57,428	**21,185**
Maximum # FIB Entries				
PrivateLarge	962,361	828,397	313,850	**18,124**
Kdl	567,009	576,274	309,575	**16,926**
PrivateSmall	38,809	49,663	21,796	**3,639**
Cogentco	38,416	60,676	30,601	**3,144**
UsCarrier	24,649	41,897	17,822	**2,234**
Colt	23,104	47,077	17,344	**3,572**
GtsCe	21,904	36,070	15,477	**2,748**
TataNld	20,736	24,776	13,179	**2,104**
DialtelecomCz	18,769	34,014	11,084	**1,393**
Ion	15,376	25,261	12,954	**1,387**
Deltacom	12,544	25,135	13,029	**1,737**
Interoute	11,881	14,182	8,346	**710**
Uninett2010	5,329	8,891	3,626	**868**

Table 6: Number of FIB entries for NCFlow vs. edge-based formulations (e.g., Fleischer-Edge), path-based formulations using Räcke Randomized Routing Trees (SMORE*), and path-based formulations using k-shortest paths (PF_4, Fleischer-Path, TEAVAR*) on every topology.

amounts of flow.

Figure 19 further breaks down the aggregate results from Figure 11 across various aspects of interest. In the two left-most columns, we break down the results by different settings of α, which illustrates how NCFlow performs on both under-subscribed ($\alpha = \{1, 8\}$) and over-subscribed ($\alpha = \{32, 64, 128\}$) traffic matrices. In the former case, NCFlow is typically able to fully satisfy the TM's requested demand, thereby matching the total flow allocated by the other methods. At the same time, NCFlow is strictly faster on all TMs, except for those belonging to smaller topologies (e.g., Uninett2010), which we discuss later on. As α increases, so, too, does NCFlow's runtime advantage; however, this does come at the cost of the total flow allocated. For example, when $\alpha = 32$, we see many instances where NCFlow is $> 100\times$ faster than PF_4, but allocates 75% of PF_4's total flow in the worst case. This effect becomes more evident for the largest settings of α: here, the speedups are $> 1000\times$, but more flow is sacrificed for some TMs. This behavior occurs perhaps because, as the traffic volume increases and the topology becomes more congested, paths that are not allowed by NCFlow's scheme become more critical for maximizing the total flow.

In the middle two columns, we break down the results by traffic model. NCFlow tends to perform best when demands are highly concentrated within clusters. In the bottom middle plot (Poisson, $\delta \to 0$), we see that NCFlow allocates $> 90\%$ of PF_4's total flow for almost every TM, while still achieving speedups $> 100\times$. Recall that as $\delta \to 0$ in the Poisson traffic model, the traffic volume *between* clusters decreases, thus generating concentrated demands. In contrast, when $\delta \to 1$, demands are less concentrated, which leads to worse performance for NCFlow in terms of total flow, but not in terms of runtime.

Finally, in the two right-most columns, we break down the results by topology size. On Uninett2010, the smallest topology in our evaluation set, NCFlow's trade-off between total flow and runtime is not much better than the other baselines, particularly Fleischer-Edge.

As the topology size increases, NCFlow's advantage becomes more apparent. On Colt, NCFlow offers faster runtimes and sacrifices little flow, no more than 10% less than PF_4. On PrivateSmall and Kdl, NCFlow's speedup increases even more: $> 100\times$ faster than PF_4 on the majority of cases on Kdl. But flow is sacrificed, particularly for large values of α. However, NCFlow's trade-off is still favorable compared to other methods: for Kdl, we see multiple instances where NCFlow achieves $1{,}000\times$ speedups at only a 20% reduction in flow. For PrivateLarge, we see both the biggest speedups and the smallest fraction of total flow relative to PF_4. As previously discussed, the outlier coincides with a highly over-subscribed TM ($\alpha = 128$). When we move to other regimes on PrivateLarge, NCFlow's performance improves: on 31 of the 400 TMs with $\alpha \in \{32, 64\}$, NCFlow is $> 1{,}000\times$ faster than PF_4 while achieving $> 80\%$ of PF_4's total flow.

In summary, we can see in this panel of CDF plots where NCFlow's strengths lie: on (1) large topologies, and (2) TMs with moderate demand volumes that are highly concentrated within the topology.

G.2 Alternate clustering methods

For each topology, we evaluate the three different clustering techniques mentioned in §3.4; on each topology we ask each technique to compute the number of clusters listed in Table 5. Figure 21 shows CDFs of the ratio of total flow and latency speed-up of a clustering technique relative to that achieved by using FMPartitioning; thus values to the left of $x = 1$ indicate worse performance compared to FMPartitioning while those on the right indicate better performance. The figure shows that clusters discovered by FM partitioning almost always let NCFlow carry more flow (red lines); using either spectral clustering or leader election leads to a noticeably smaller allocation in about 20% and 40% of the cases. The figure shows a less clear-cut separation on latency speed-up; clusters discovered by leader election offer more speedup in over 30% of the experiments. Overall, we see that FMPartitioning performs better on average but not in all cases.

G.3 Effect on path latency

Figure 22 shows a CDF of the *normalized path latency* for de-

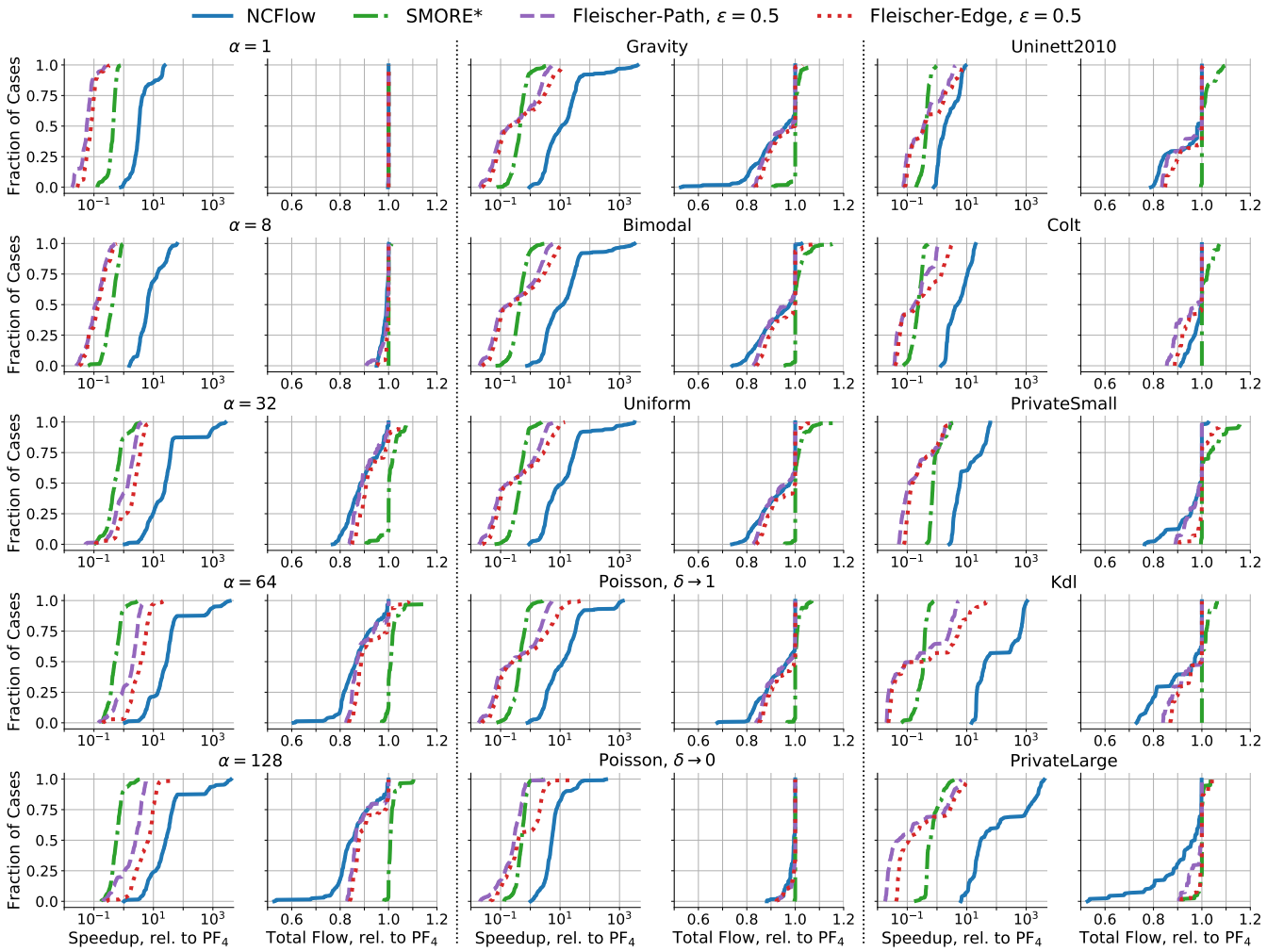

Figure 19: A breakdown of the experimental results from Figure 11 along various dimensions of interest: scale factor, traffic model, and topology size. NCFlow excels on large topologies with TMs that have highly concentrated demands.

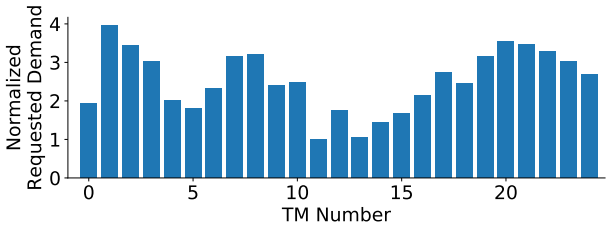

Figure 20: Traffic demand for each traffic matrix used in the demand tracking experiment (see Figure 15) on PrivateLarge. The exact values are not shown for confidentiality reasons.

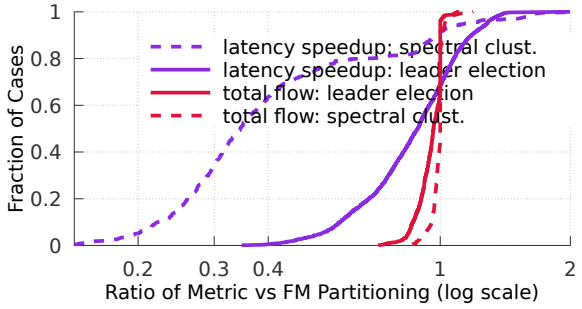

Figure 21: Comparing the total flow allocated and the speedup in computing allocations when clusters are chosen using the three techniques mentioned in §3.4–FM partitioning, spectral clustering and leader election. The default technique used in our evaluation, FM partitioning, generally performs better but not in all cases.

mands[6] under different flow allocations. The figure on the top shows CDFs of the actual normalized path latency. Observe that these distributions are nearly identical. The figure on the bottom shows a CDF of the ratio of normalized latency; we see that roughly 70% of the demands are carried by NCFlow on paths that are at most as long as the paths used by PF_4 (i.e., to the left of x=1). Most of the cases where NCFlow uses

[6]The latency of the paths along which each demand is routed weighted by the fraction of the demand routed along each path. That is, if a demand is divided equally between two paths, the normalized latency will be the average of the path latencies.

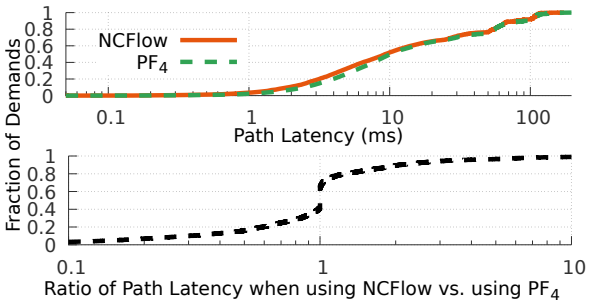

Figure 22: Effect of NCFlow on path latency

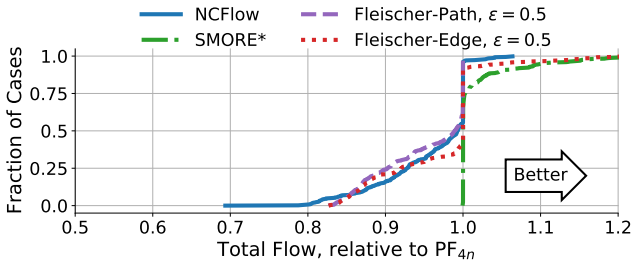

(a) CDF of total flow relative to PF_{4n}

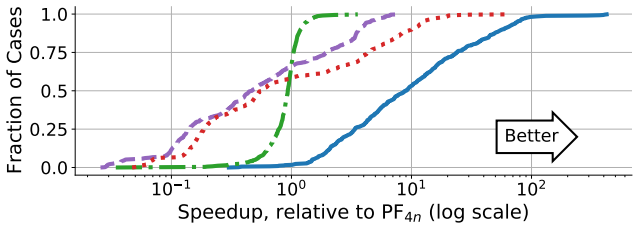

(b) CDF of speedup relative to PF_{4n}

Figure 23: Similarly to Figure 11 all schemes use up to $k = 4$ shortest paths between each pair of nodes except that the paths are chosen *without* ensuring edge disjointness. The figure shows no qualitative difference relative to Figure 11.

relatively longer paths are for demands that have very small latency paths as illustrated by the top figure.

Note that path latency can be further explicitly controlled in NCFlow by determining which paths can be used or by weighting the objective to prefer shorter paths in the various steps of Figure 6.

G.4 Alternate path choices

With Figure 23, Figure 24, Figure 25, Figure 26, Figure 27 we evaluate different numbers of paths between node pairs chosen with or without edge disjointness. PF_k refers to path formulation with k shortest paths chosen using edge disjointness and PF_{kn} indicates paths chosen without edge disjointness. Comparing these figures with Figure 11, we note that NCFlow's improvements over baselines hold across different path choices.

Note that Figure 26 and Figure 27 are missing some of the larger topologies listed in Table 5 for some of the baseline schemes because the baselines ran out of memory (we used a server with up to 3TB of memory) or raised some other exception.

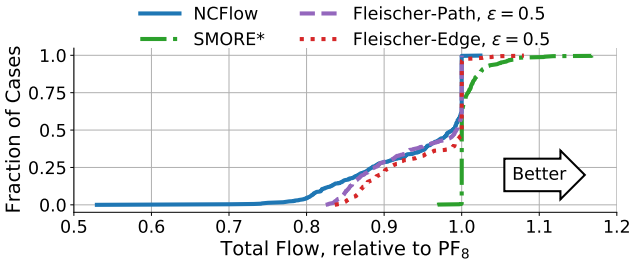

(a) CDF of total flow relative to PF_8

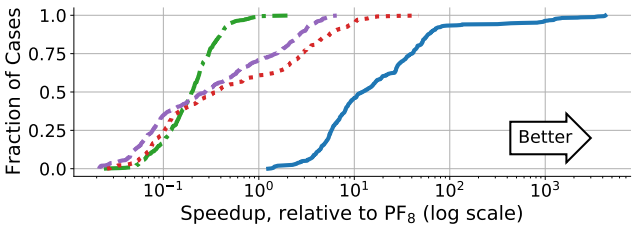

(b) CDF of speedup relative to PF_8

Figure 24: Similar to Figure 11 except all schemes use up to $k = 8$ shortest paths between each pair of nodes; paths chosen *with* edge disjointness. The figure shows no qualitative difference relative to Figure 11.

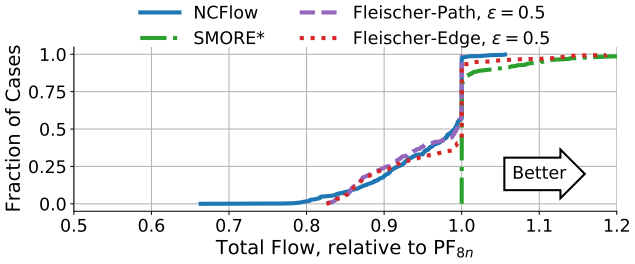

(a) CDF of total flow relative to PF_{8n}

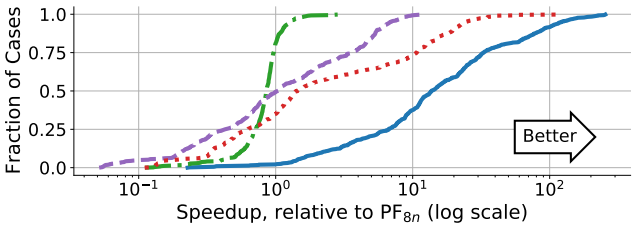

(b) CDF of speedup relative to PF_{8n}

Figure 25: Similar to Figure 11 except all schemes use up to $k = 8$ shortest paths between each pair of nodes; paths chosen *without* ensuring edge disjointness. The figure shows no qualitative difference relative to Figure 11.

H Illustrative examples

Here, we show some illustrative examples where applying NCFlow using adversarially chosen clusters can lead to sub-optimal flow allocation.

Figure 28 shows a case wherein NCFlow is sub-optimal because the aggregate graph (wherein nodes are clusters) is

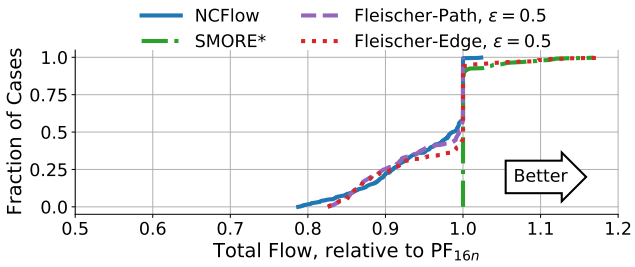

(a) CDF of total flow relative to PF_{16n}

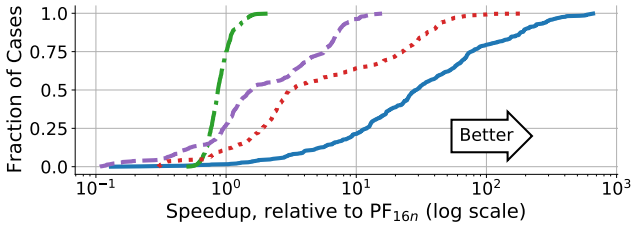

(b) CDF of speedup relative to PF_{16n}

Figure 26: Similar to Figure 11 except all schemes use up to $k = 16$ shortest paths between each pair of nodes; paths chosen *without* ensuring edge disjointness. The figure shows no qualitative difference relative to Figure 11.

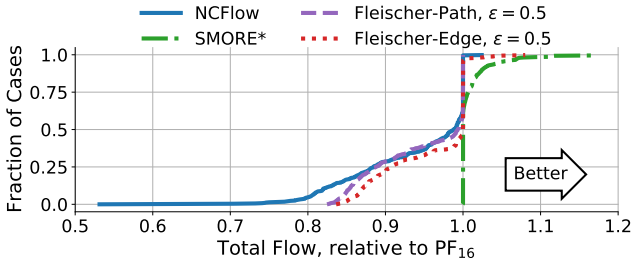

(a) CDF of total flow relative to PF_{16}

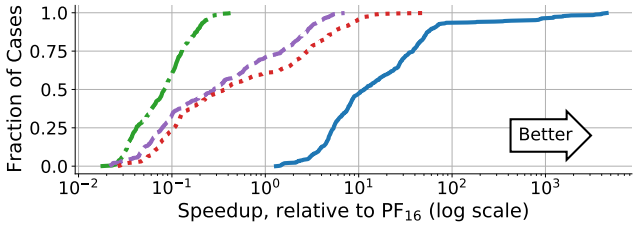

(b) CDF of speedup relative to PF_{16}

Figure 27: Similar to Figure 11 except all schemes use up to $k = 16$ shortest paths between each pair of nodes; paths chosen *with* ensuring edge disjointness. The figure shows no qualitative difference relative to Figure 11.

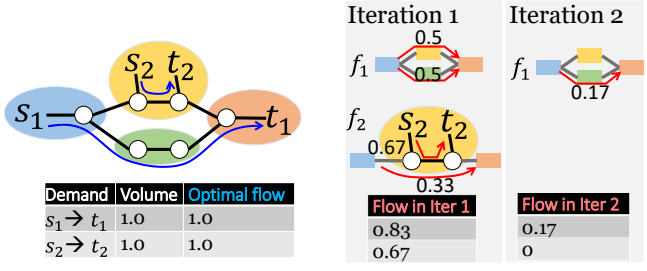

Figure 28: Sub-optimality of NCFlow when the aggregate graph is not a tree.

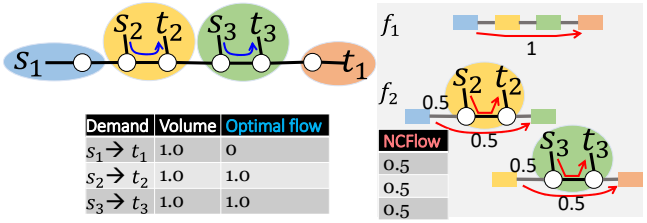

Figure 29: Sub-optimality of NCFlow when demands cannot be fully satisfied.

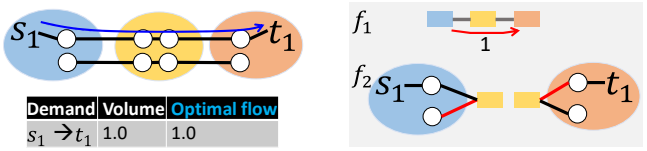

Figure 30: Sub-optimality of NCFlow when there are multiple-edges between pairs of clusters.

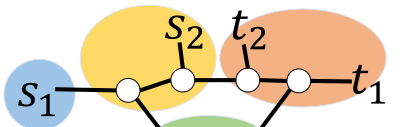

(a) For the suboptimality problem in Figure 28, a different clustering choice that leads to optimal flow allocation with NCFlow.

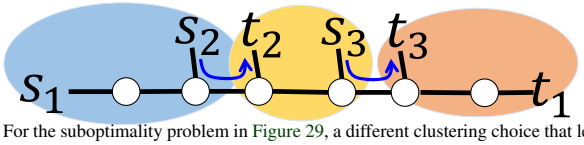

(b) For the suboptimality problem in Figure 29, a different clustering choice that leads to optimal flow allocation with NCFlow.

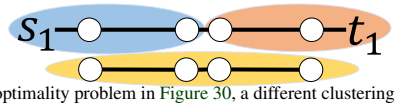

(c) For the suboptimality problem in Figure 30, a different clustering choice that leads to optimal flow allocation with NCFlow.

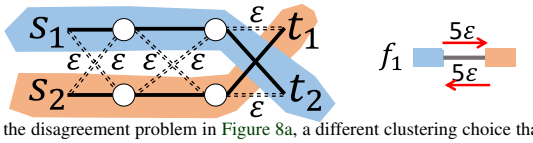

(d) For the disagreement problem in Figure 8a, a different clustering choice that does not lead to such a disagreement.

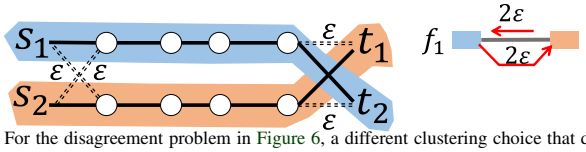

(e) For the disagreement problem in Figure 6, a different clustering choice that does not lead to such a disagreement.

Figure 31: Alternate clustering choices that fix suboptimality concerns and disagreements.

not a tree. The network topology and optimal allocations are shown in the graph on the left; assume each link has a unit capacity. With NCFlow, as shown in the figures on the right, MaxAggFlow can route the flow from s_1 to t_1 on either the top or the bottom path or divide between the two paths in some proportion; note that MaxAggFlow is not aware of demands

that are local to a cluster (such as the flow from s_2 to t_2). Whenever MaxAggFlow assigns non-zero flow for the $s_1 \to t_1$ demand on the top path, NCFlow will be sub-optimal because then the other demand cannot be fully satisfied when MaxClusterFlow executes later on the yellow cluster. Any unsatisfied volume for $s_1 \to t_1$ can be routed on the bottom path in a later iteration but the flow for $s_2 \to t_2$ will not increase since the links that demand can use are fully utilized in the first iteration. The root of the problem here is that MaxAggFlow allocates traffic over multiple paths without being aware of the demands within clusters.

Figure 29 shows a case wherein NCFlow is sub-optimal when demands cannot be fully satisfied. As above, the topology and optimal allocations are shown on the left. Also, as above, the root of the issue here is that MaxAggFlow allocates the cross-cluster flow on the aggregate graph without being aware of the demands within clusters. As shown, subsequently, MaxClusterFlow will under-allocate flow for the local demands even though total flow would be larger if the local demands are fully satisfied.

Reordering the sub-problems, i.e., executing MaxClusterFlow before MaxAggFlow, may appear promising based on these examples but simple counter-examples exist even for such a reordered solution. The underlying cause of sub-optimality is not the order in which the global and local solutions are computed but rather that the optimal flow allocation requires *jointly solving* these problems.

Figure 30 shows a case wherein NCFlow can be sub-optimal when multiple edges connect clusters. As above, each unmarked link has unit capacity and the optimal allocations are shown in blue. Recall that NCFlow uses exactly one edge between each pair of clusters per iteration to avoid disagreements. There are two edges between each cluster but among the four possible crossing edge choices in an iteration, exactly one choice can carry non-trivial amount of flow (the top edge for each cluster pair). If that choice is somehow not picked, as shown marked in red on the right in Figure 30, NCFlow will not satisfy the demand. Simply increasing the number of iterations may not suffice either since the number of edge choices can be large, depending on the path lengths on the aggregate graph and on the number of edges between clusters.

As noted previously, the above examples are in part due to poor cluster choices; Figure 31 shows different cluster choices for these examples under which NCFlow will lead to optimal flow allocation.

I Optimality gap

$u_e, v_e \in \mathcal{V}$	Edge $e \in \mathcal{E}$ goes from node u_e to node v_e
$m_u, \forall u \in \mathcal{V}$	m_u denotes the cluster containing node u. Note that $m_u \in \mathcal{V}_{\text{agg}}$ (i.e., the cluster is a node on the aggregate graph) and $u \in \mathcal{V}_{m_u}$ (i.e., the node u belongs in the restricted graph for the m_u'th cluster)
$\forall k \in \mathcal{D}, m_{s_k} \neq m_{t_k}, x \in \mathcal{V}_{\text{agg}}$	
$\mathsf{OutNodes}(x,k)$	The nodes in cluster x that can carry flow of demand k *out to* some other cluster, i.e., $\{u \mid m_u = x, \exists v \in \mathcal{V}, p \in \mathcal{P}_{\text{agg},K_{s_k t_k}}$ s. t. $m_v = y, (x,y) \in p, (u,v) \in \mathcal{E}\}$
$\mathsf{InNodes}(x,k)$	The nodes in cluster x that can carry flow of demand k *into* cluster x, i.e., $\{u \mid m_u = x, \exists v \in \mathcal{V}, p \in \mathcal{P}_{\text{agg},K_{s_k t_k}}$ s. t. $m_v = y, (y,x) \in p, (v,u) \in \mathcal{E}\}$

Table 7: Additional notation for optimality gap; builds on top of notation from Table 2 and Table 3.

$$\mathsf{MaxEdgeFlow}(\mathcal{V},\mathcal{E},\mathcal{D}) \triangleq \arg\max_{\mathbf{f}} \sum_{k\in\mathcal{D}} f_k \text{ s.t.} \tag{6}$$

$$\mathbf{f} = \left\{ f_{ke} \mid \forall k \in \mathcal{D}, e \in \mathcal{E} \right\} \quad \text{and}$$

$$f_{ke} \geq 0 \qquad \forall e \in \mathcal{E}, k \in \mathcal{D} \quad \text{(non-negative flow)}$$

$$f_k \leq d_k, \qquad \forall k \in \mathcal{D} \quad \text{(below volume)}$$

$$\sum_{\forall k,e} f_{ke} \leq c_e, \qquad \forall e \in \mathcal{E} \quad \text{(below capacity)}$$

$$\sum_{e,u_e=u} f_{ke} - \sum_{e,v_e=u} f_{ke} = \begin{cases} f_k & \text{if } u = s_k \\ -f_k & \text{if } u = t_k \ \forall k \in \mathcal{D}, u \in \mathcal{V} \\ 0 & \text{o/w.} \end{cases} \quad \text{(flow cnsrvtn.)}$$

I.1 Optimal MaxEdgeFlow

The optimal flow allocation algorithm, in terms of carrying the maximum amount of flow possible on a network, is as shown in Equation 6. We will call this the EF, short for MaxEdgeFlow. Some additional notation is in Table 7. Observe that, in this formulation, any demand can be allocated on any edge (the variable f_{ke}) as long as flow conservation holds (the longer equation at the bottom). As noted in §2, this *edge-form* of the problem carries the maximal amount of flow but has a high computation time and requires a large number of forwarding entries at switches (one rule per nodepair at each node).

I.2 Edge flow with cluster constraints

Relative to the optimal MaxEdgeFlow, we first ask how much flow will be lost by using clusters. To compute this value, we add to MaxEdgeFlow the constraint shown in Equation 7. Specifically, demands whose source and target are in the same cluster can only use edges within the cluster. However, as above, paths remain otherwise unconstrained.

$$f_{ke} = 0 \ \ \forall e, u_e \notin \mathcal{V}_x \text{ or } v_e \notin \mathcal{V}_x, \text{ if } m_{s_k} = m_{t_k} = x. \tag{7}$$

We will call this optimization problem EF with cluster constraints.

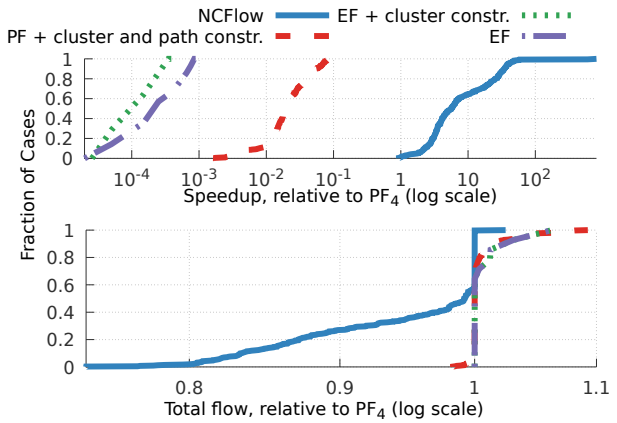

Figure 32: Comparing flow allocated by NCFlow with the best possible flows

I.3 Path form with cluster and path constraints

Next, we ask how much flow will be lost when using the clusters as well as the given set of paths within and between clusters? Computing this value is somewhat more complex because we have to stitch together the flow carried on paths within each cluster with the flow on the edges between clusters while also ensuring that flow follow the chosen paths on the aggregate graph (where clusters are nodes). For reference, we write this out in Equation 8.

In more detail, this optimization problem, as shown in Equation 8, has three classes of decision variables – f_K^p, f_k^p, f_{ke} – which respectively are the flow allocated to a bundled demand on a path on the aggregate graph, the flow allocated to a demand on a path within a cluster and the flow allocated to a demand on a crossing edge between clusters.

Equation 9 computes the net flow for each demand k which for the case of a demand whose source and target are in the same cluster is the sum of flow carried on all intra-cluster paths. For demands whose source and target are in different clusters, the net flow is the flow from the demand's source to all of the nodes in the source's cluster that connect with other clusters as well as the flow to the demand's target from all of the nodes in the target's cluster that connect with other clusters.

For flow conservation, consider Equation 11 which ensures that all of the flow leaving at a node u for a demand k on crossing edges to other clusters equals the flow that comes into the node u either from the source of the demand (if the source is within its cluster) or from all of the nodes in u's cluster that can receive flow for demand k from other clusters– $\mathsf{InNodes}(m_u, k)$. Equation 12 considers the converse case for demands that leave at a node. Finally, Equation 13 relates the total flow between a pair of clusters x, y on the crossing edges between these clusters with the flow along paths on the aggregate graph that contain the edge (x, y). We will call this optimization problem PF with cluster and path constraints.

Note that the above constraints naturally lead to a reduction in forwarding table size as discussed in §3.5. However, it is not clear how much less flow these constraints allow for relative to the optimal EF. Moreover, since this optimization has more variables (and constraints) than PF_4 (see Equation 2), it can take longer to compute and may not be practically useful. We use this optimization problem to discern how much flow is lost by the constraints used in NCFlow (restricting to clusters and paths) relative to the flow that is lost due to the heuristic allocation process described in §3.

I.4 Experimental results

Our results are in Figure 32; the baseline is PF_4 and the figures plot CDFs of total flow and latency speedup for many topologies and traffic demands. Note that using the edge formulation (purple dash-dots) often leads to substantially more flow being allocated compared to PF_4; however, as the figure on the top shows, edge formulation is a more complex problem that takes longer to run (over $1000\times$ longer).

Adding the clustering constraint to edge formulation has an un-noticeable effect on the flow allocation (green dashes). Note that we use clusters computed using FMPartitioning for all topologies.

Constraining the path formulation using both the given clusters and the given paths (between clusters and within each cluster), as shown with the red dash line, allocates much more flow than PF_4 and not much less than is allocated in edge formulation. Thus, empirically, constraining flow allocation to traverse the chosen clusters and paths does not limit the flow that can be allocated. The figure also shows that computing the optimal flow given clusters and paths takes longer than PF_4 (roughly $10\times$ – $100\times$ longer). Thus, NCFlow offers a heuristic which finishes substantially faster than PF_4.

To sum up, our two main contributions are: (1) constraining flow allocations to use specific clusters and paths which reduces the number of forwarding table entries needed without affecting the flow that can be allocated and (2) a heuristic that computes flow allocations quickly given this constraint but can under-allocate flow. We believe that future work can improve the heuristic to reduce the flow loss further.

$$\mathsf{MaxClusterPathFlow}(\mathcal{V},\mathcal{E},\mathcal{D},\mathcal{P}) \triangleq \arg\max_{\mathbf{f}} \sum_{k\in\mathcal{D}} f_k \qquad \text{s.t.} \tag{8}$$

$$\mathbf{f} = \Big\{ f_K^p \mid \forall K \in \mathcal{D}_{\text{agg}}, p \in \mathcal{P}_{\text{agg}}, \quad \text{(flow on inter-cluster paths)}$$
$$f_k^p \mid \forall k \in \mathcal{D}, p \in \mathcal{P}, \quad \text{(flow on intra-cluster paths)}$$
$$f_{ke} \mid \forall k \in \mathcal{D}, e \in \mathcal{E}, m_{u_e} \neq m_{v_e} \text{(flow on edges between clusters)} \Big\}$$

and

$$f_k = \begin{cases} \sum\limits_{p\in\mathcal{P}_{s_k,t_k}} f_k^p & \text{if } m_{s_k} = m_{t_k} \quad \text{(flow within a cluster)} \\ \sum\limits_{t\in\mathsf{OutNodes}_{(m_{s_k},k)}} \sum\limits_{p\in\mathcal{P}_{s_k,t}} f_k^p & \text{if } m_{s_k} \neq m_{t_k} \quad \text{(flow from source to outnodes)} \\ \sum\limits_{s\in\mathsf{InNodes}_{(m_{t_k},k)}} \sum\limits_{p\in\mathcal{P}_{s,t_k}} f_k^p & \text{if } m_{s_k} \neq m_{t_k} \quad \text{(flow to target from innodes)} \end{cases} \qquad \forall k \in \mathcal{D}\text{(net flow)} \tag{9}$$

$$f_k \leq d_k \text{(flow below volume)} \qquad \forall k \in \mathcal{D}$$

$$c_e \geq \begin{cases} \sum\limits_{k\in\mathcal{D}} \sum\limits_{p\in\mathcal{P},\ p\ni e} f_k^p & \text{if } m_{u_e} = m_{v_e} \quad \text{(intra-cluster edges; note: } k \text{ goes over all demands)} \\ \sum\limits_{k\in\mathcal{D}} f_{ke} & \text{otherwise} \quad \text{(inter-cluster edges)} \end{cases} \qquad \forall e \in \mathcal{E}, \tag{10}$$

$$\sum_{e\in\mathcal{E}|u_e=u,\ m_{u_e}\neq m_{v_e}} f_{ke} = \begin{cases} \sum\limits_{p\in\mathcal{P}_{s_k,u}} f_k^p & \text{if } m_u = m_{s_k} \quad \text{(at cluster } m_u\text{, flow from } s_k \text{ to } u\text{)} \\ \sum\limits_{v\in\mathsf{InNodes}(m_u,k)} \sum\limits_{p\in\mathcal{P}_{v,u}} f_k^p & \text{otherwise} \quad \text{(at cluster } m_u\text{, flow from all } \mathsf{InNodes} \text{ to } u\text{)} \end{cases} \qquad \forall u \in \mathcal{V}, k \in \mathcal{D} \tag{11}$$

$$\sum_{e\in\mathcal{E}|v_e=u,\ m_{u_e}\neq m_{v_e}} f_{ke} = \begin{cases} \sum\limits_{p\in\mathcal{P}_{u,t_k}} f_k^p & \text{if } m_u = m_{t_k} \quad \text{(at cluster } m_u\text{, flow from } u \textbf{ to } t_k\text{)} \\ \sum\limits_{v\in\mathsf{OutNodes}(m_u,k)} \sum\limits_{p\in\mathcal{P}_{u,v}} f_k^p & \text{otherwise} \quad \text{(at cluster } m_u\text{, flow from } u \text{ to all } \mathsf{OutNodes}\text{)} \end{cases} \qquad \forall u \in \mathcal{V}, k \in \mathcal{D} \tag{12}$$

$$\sum_{p\in\mathcal{P}_{\text{agg}}|(x,y)\in p} f_K^p = \sum_{e|m_{u_e}=x,\ m_{v_e}=y,\ k\in K} f_{ke} \qquad \forall K \in \mathcal{D}_{\text{agg}},\ x,\ y \in \mathcal{V}_{\text{agg}} \quad \text{(flow b/w clusters = flow on inter-cluster path)} \tag{13}$$